Higher-seniority excitations in even neutron-rich Sn isotopes

Ł. W. Iskra,[1] R. Broda,[1] R. V. F. Janssens,[2] J. Wrzesiński,[1] B. Szpak,[1] C. J. Chiara,[2,3] M. P. Carpenter,[2] B. Fornal,[1] N. Hoteling,[2,3] F. G. Kondev,[4] W. Królas,[1] T. Lauritsen,[2] T. Pawłat,[1] D. Seweryniak,[2] I. Stefanescu,[2,3] W. B. Walters,[3] and S. Zhu[2]

[1]*Institute of Nuclear Physics, Polish Academy of Sciences, PL-31342 Kraków, Poland*
[2]*Physics Division, Argonne National Laboratory, Argonne, Illinois 60439, USA*
[3]*Department of Chemistry and Biochemistry, University of Maryland, College Park, Maryland 20742, USA*
[4]*Nuclear Engineering Division, Argonne National Laboratory, Argonne, Illinois 60439, USA*

(Received 26 February 2014; published 28 April 2014)

Excited states above the seniority $\nu = 2$ isomers have been investigated in even neutron-rich $^{118-128}$Sn isotopes produced by fusion-fission of 6.9 MeV/A ^{48}Ca beams with ^{208}Pb and ^{238}U targets and by fission of 6.7 MeV/A ^{64}Ni beams on a ^{238}U target. Level schemes up to excitation energies in excess of 8 MeV have been established based on multifold γ-ray coincidence relationships measured with the Gammasphere array. Isotopic identification of crucial transitions was achieved through a number of techniques, including prompt and delayed cross-coincidence methods. As a result, seniority $\nu = 4$, 15^-, and 13^- isomers were observed and their half-lives determined. These long-lived states in turn served as steppingstones to delineate the isomeric decays and to locate higher-lying states with good sensitivity. As the observed isomeric decays feed down to 10^+ and 7^- isomers, firm spin-parity assignments could be proposed for most of the seniority $\nu = 4$ states. Higher-lying, seniority $\nu = 6$ levels were assigned tentatively on the basis of the observed deexcitation paths as well as of general yrast population arguments. Shell-model calculations were carried out down to ^{122}Sn in the $g_{7/2}$, $d_{5/2}$, $d_{3/2}$, $s_{1/2}$, and $h_{11/2}$ model space of neutron holes with respect to a ^{132}Sn core. Effective two-body interactions were adjusted such that satisfactory agreement with data was achieved for ^{130}Sn. The results reproduce the experimental level energies and spin-parity assignments rather well. The intrinsic structure of the states is discussed on the basis of the calculated wave functions which, in many instances, point to complex configurations. In a few cases, the proposed assignments lead to unresolved issues. The smooth, systematic decrease of the level energies with mass A is accompanied by the similarly regular behavior with A of the reduced transition probabilities extracted from the isomeric half-lives. This A dependence is discussed for the $E1$ and $E2$ transitions in the decay of the seniority $\nu = 4$ isomers and is compared to that determined in earlier work for the $E2$ transition rates from the $\nu = 2,3$ isomers.

DOI: 10.1103/PhysRevC.89.044324 PACS number(s): 23.20.Lv, 21.60.Cs, 27.60.+j, 25.70.Jj

I. INTRODUCTION

Protons in the $N = 82$ isotones and neutrons in the $Z = 50$ isotopes are filling the $g_{7/2}$, $d_{5/2}$, $s_{1/2}$, $d_{3/2}$, and $h_{11/2}$ single-particle levels distributed between the major shells with neutron and proton numbers 50 and 82. Whereas, for protons, a sizable energy separation of the last three orbitals from the first two gives rise to a $Z = 64$ subshell closure and results in the apparent magicity of ^{146}Gd$_{82}$ [1], in the even Sn isotopes the energy of the first excited 2^+ state (2_1^+) is stable and ^{114}Sn$_{64}$ does not exhibit any discontinuity in its level structure. Despite this difference, for both protons and neutrons, the high-j, $h_{11/2}$ intruder orbital largely determines the structure of yrast levels in nuclei above $Z = 64$ and $N = 64$, respectively. A characteristic feature is the appearance of isomeric states, in particular of 10^+ and $27/2^-$ $(h_{11/2})^n$ seniority-2 and -3 isomers, and these have been established in all of the even and odd $N = 82$ isotones and $Z = 50$ isotopes [2–7], respectively. For protons, these isomers have been studied with standard fusion-evaporation reactions up to the most proton-rich, $Z = 72$, ^{154}Hf nucleus [8]. The smooth variation with Z of the $B(E2)$ reduced transition probabilities, extracted for the isomeric transitions, reflects the filling of the proton $h_{11/2}$ subshell: The half filling was determined to occur for the $Z = 71$, ^{153}Lu nucleus where the isomeric decay has the lowest $B(E2)$ value [8]. The same phenomenon was studied even more extensively for neutrons in a series of experiments exploiting deep-inelastic reactions with heavy ions to produce the neutron-rich Sn isotopes of interest [4–6]. In this case, the systematics of the corresponding $B(E2)$ probabilities established the $N = 73$, ^{123}Sn isotope as the nucleus with a half-filled $h_{11/2}$ subshell [5,6].

These rather striking shell-model features raised interest in investigating the role of the $h_{11/2}$ subshell in higher-seniority excitations. For protons, the study of ^{150}Er in Ref. [9] provided the identification of the $(h_{11/2})^4$ and $(h_{11/2})^3 d_{3/2}$ seniority-4 excitations up to the 16^+ and 15^- highest-spin levels, respectively. However, such investigations have not been extended to higher-Z, $N = 82$ isotones and, for neutrons, until recently no experimental information was available on levels located above the seniority-2 and -3 isomers in the Sn isotopic chain. In this work, results of such a study are presented for the neutron-rich, even Sn isotopes produced in fusion-fission reactions and analyzed using high-fold, γ-ray coincidence data obtained in several experiments performed with the Gammasphere multidetector array. While the present investigation was ongoing, two other groups independently performed parallel research with the same goal, and their results were reported recently [10,11]. Fotiades *et al.* [10]

analyzed data from three different fusion-fission reactions as well as from separate measurements with (n,xn) reactions on stable Sn monoisotopic targets to identify crucial yrast transitions above the 10^+ isomers. This group reported rather rudimentary level schemes including only the three or four most intense transitions in the ^{120,122,124}Sn isotopes, but established a considerably more complete level scheme above the 10^+ long-lived state in ^{118}Sn. However, Astier *et al.* [11] reported fairly complete level schemes in all even- and odd-Sn isotopes from $A = 119$ to 126 as populated in $^{12}\mathrm{C} + ^{238}\mathrm{U}$ and $^{18}\mathrm{O} + ^{208}\mathrm{Pb}$ fusion-fission reactions. Though the results of the present study overlap to a large extent with the findings of Astier *et al.*, they were obtained prior to the publication of Ref. [11] in experiments using different reactions. In some instances the approach to the analysis was also different. Apart from the comforting similarity of the results obtained in independent experimental efforts, the level schemes reported here are often more detailed, especially in instances which may turn out to be critical for the interpretation of some of the observed structures. In addition, the 15^- isomer in neutron-rich ^{128}Sn was also identified recently, following a fragmentation reaction [12]. Although the very small production yield of this isotope in the fusion-fission reactions used here did not allow to add further information to the ^{128}Sn level scheme, the presence of this new 15^- isomer was confidently confirmed, herewith extending the systematics of 15^- isomers established in the Sn isotopic chain. Only the results obtained for even Sn isotopes in the $A = 118$–128 mass range are presented here. A separate paper describing the recently completed investigation of odd-Sn isotopes will soon follow [13].

II. EXPERIMENTAL PROCEDURES AND DATA ANALYSIS

The data for the present study were obtained in three experiments devoted originally to investigations of neutron-rich Ni [14] and K [15,16] nuclei produced in deep-inelastic reactions (a general description of the technique can be found in Ref. [17]). These measurements were all performed at Argonne National Laboratory with the ATLAS superconducting linear accelerator and the Gammasphere [18] array consisting of 101 Compton-suppressed high-purity Ge detectors. Standard, three- and higher-fold γ-ray coincidence data were recorded for all reactions taking place in 330-MeV $^{48}\mathrm{Ca} + ^{208}\mathrm{Pb}$, 330-MeV $^{48}\mathrm{Ca} + ^{238}\mathrm{U}$, and 430-MeV $^{64}\mathrm{Ni} + ^{238}\mathrm{U}$ collisions. In all three experiments, described in detail elsewhere [14–16], the $\sim$50 mg/cm^2 ^{208}Pb and ^{238}U targets were of sufficient thickness to stop both the reaction products and the ^{48}Ca and ^{64}Ni beams. The latter were pulsed with a 412-ns repetition rate and an intrinsic pulse width of $\sim$0.3 ns. These conditions enabled a clean separation between prompt (P) and delayed (D) coincidence events which could be sorted into (PPP) and (DDD) cubes as well as in a variety of (PDD) and (PPD) histograms with time conditions optimized for specific isomeric half-lives in each of the Sn isotopes of interest. Further details about the analysis techniques can be found in Refs. [14–16] and the references therein.

As demonstrated in Fig. 1, a very similar range of neutron-rich Sn isotopes was populated by the three reactions,

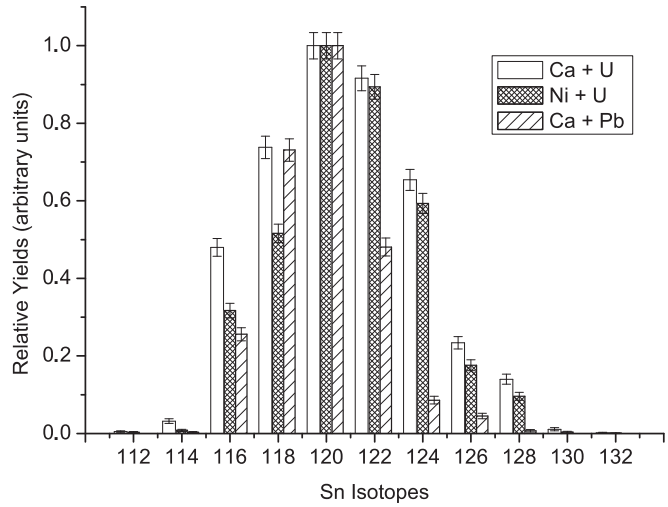

FIG. 1. Relative yields of the Sn isotopes produced in $^{48}\mathrm{Ca} + ^{238}\mathrm{U}$, $^{64}\mathrm{Ni} + ^{238}\mathrm{U}$, and $^{48}\mathrm{Ca} + ^{208}\mathrm{Pb}$ reactions as indicated. In each case, the delayed γ coincidence data were used to determine the summed population intensity of all isomers.

and the complementary analysis of the various data sets provided numerous opportunities to cross-check and verify the experimental findings.

The coincidence analyses established unambiguously Te and Sm nuclei as the fission partners of the Sn isotopes in $^{48}\mathrm{Ca} + ^{208}\mathrm{Pb}$ and $^{48}\mathrm{Ca} + ^{238}\mathrm{U}$ reactions, respectively. Thus, fusion-fission is the primary production process of the neutron-rich Sn isotopes in these two systems. Figure 2 displays the distribution of the number of neutrons evaporated in the $^{48}\mathrm{Ca} + ^{208}\mathrm{Pb}$ (a) and $^{48}\mathrm{Ca} + ^{238}\mathrm{U}$ (b) fusion-fission reactions, as extracted from the cross-coincidence analyses between the fission fragments. This distribution indicates that the fission process occurred from compound nuclei with high excitation energy leading to the evaporation of large numbers of neutrons, presumably in prefission processes, or from the highly excited secondary fragments themselves. However, in the $^{64}\mathrm{Ni} + ^{238}\mathrm{U}$ reaction, the Yb transitions expected in cross coincidence with the Sn γ rays were *not* observed, indicating that fusion did not take place. Rather, the presence of coincident Mo transitions indicated that, in this case, fission occurred directly from the

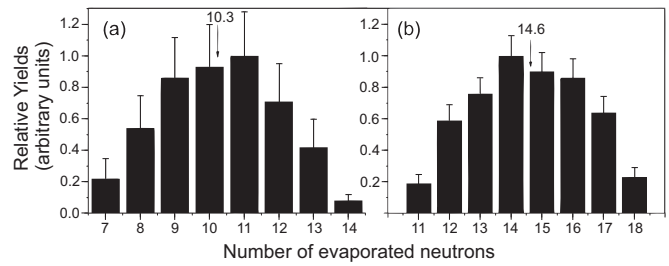

FIG. 2. Distributions of the number of neutrons evaporated in the $^{48}\mathrm{Ca} + ^{208}\mathrm{Pb}$ (a) and $^{48}\mathrm{Ca} + ^{238}\mathrm{U}$ (b) fusion-fission reactions obtained from the mass balance between the Sn isotopes and the respective complementary Te (a) and Sm (b) fragments as determined in the cross-coincidence analysis described in the text.

^{238}U target and, possibly, also from excited targetlike reaction products. This clarification of the various reaction processes was reported earlier [19] and was found to be necessary when cross-coincidence analyses proved to be crucial to identify transitions in Sn isotopes located above long-lived isomers (see below).

For ^{118,120,126}Sn, the respective $T_{1/2} = 2.5$-, 6.3-, and 7.7-μs half-lives [3,6,7] of the 10^+ isomers turned out to be sufficiently short to identify the most intense transitions above these long-lived states through the analysis of coincidence spectra obtained with delayed gates placed on known γ rays in the corresponding decays. However, in practice, in ^{120}Sn and ^{126}Sn the long-lived 7^- isomers excluded the possibility to observe delayed coincidences with lower-lying transitions and this identification of γ rays from higher-lying levels had to be based solely on the respective $(8^+ \rightarrow 7^-)$ transition. As a result, additional supporting evidence required a more complex analysis of cross-coincidence relationships with γ rays from the complementary fission fragments. The latter method was essentially the only one applicable to the case of ^{122}Sn and ^{124}Sn, where the longer half-lives of the 10^+ isomers ($T_{1/2} = 62$ and 45 μs, respectively [4]) excluded the delayed-coincidence technique. With the exception of ^{118}Sn, the presence of higher-lying isomers was established in all other even Sn isotopes under investigation. In each case, the decay occurs via a cascade of three transitions to the corresponding 10^+ long-lived state. In turn, these new isomers, all with half-lives suitable for an efficient analysis of selected PDD and PPD histograms, provided the basis for the extension of the level schemes towards higher excitation energy ($\sim$7 MeV). First, the prompt (P) coincidence spectra obtained from the PDD cubes with two delayed (DD) gates placed on the three intense γ transitions from the decays of the new isomers enabled the identification of all the higher-lying transitions in each Sn isotope. Subsequently, the higher parts of these level schemes were developed based on PP coincidence matrices obtained from the PPD cubes by selecting any of the three strong, delayed (D) transitions below the respective isomers. Finally, the process could be reversed: By selecting in the PDD and PPD cubes one or two prompt (P) transitions linking the higher-lying levels, clean delayed D coincidence spectra and DD matrices were obtained. From the latter histograms, additional deexcitation paths from the new isomers were unambiguously established. In some cases, the presence of sequential isomeric decays was exploited to obtain clean spectra from ddD cubes, where all three γ rays are delayed, but where the third one (D) is delayed with respect to the two others (dd). In a last step, the detailed inspection of the DDD coincidences completed the analysis. The results are presented below. However, in view of the recent works of Refs. [10,11], only a summary is presented here with an emphasis on new findings.

III. RESULTS

In the level schemes presented below, spin-parity assignments are based on combined considerations taking into account γ decays toward states assigned in earlier work, systematics, yrast feeding arguments, measured state half-lives, and comparisons with theory. In some instances, assignments were supported further by angular-correlation and intensity-balance data from Ref. [11]. For each nucleus below, these assignments are discussed toward the end of the individual subsections, even though the assigned spins and parities are used throughout the entire discussion for clarity.

A. ^{118}Sn

The 2.5-μs and 230-ns half-lives of the 10^+ and 7^- isomers in ^{118}Sn enabled the use of standard delayed-coincidence techniques while ensuring that good selectivity was achieved for the identification of higher-lying transitions. A spectrum presenting these γ rays is displayed in Fig. 3(a): It was obtained by placing double coincidence gates on all combinations of the four strongest transitions associated with the 10^+ isomeric decay in the summed PDD data from the three experiments. In this spectrum, ^{118}Sn transitions identified as preceding in time both isomers are marked by open circles, while all other, unlabeled lines arise from identified cross-coincidence relationships with the accompanying fragment nuclei and/or from $(n,n'\gamma)$ background. The intense 477-keV line corresponds to the $8^+ \rightarrow 7^-$ transition which is strongly populated in the 10^+ decay and precedes in time the 7^- isomer (see Fig. 4). In a more detailed analysis, strong feeding of the 7^- isomer was established through a family of five additional transitions that have no visible connection to the 10^+ long-lived state. This is documented through the two lower spectra of Fig. 3. Panel (b) was obtained by placing a gate on the most intense prompt 1238-keV transition above the 10^+ isomer in the PD matrix and the four observed delayed lines are representative of the coincidence relationships observed for most of the newly identified γ rays; i.e., in addition to the 477-keV, $8^+ \rightarrow 7^-$ transition, three other strong lines are present at 254 $(7^- \rightarrow 5^-)$, 1051 $(4^+ \rightarrow 2^+)$, and 1230 $(2^+ \rightarrow 0^+)$ keV from the decay of the 7^- long-lived state. In the delayed spectrum of Fig. 3(c), with gates placed on the prompt 778- and 1018-keV γ rays, the 477-keV line is notably absent while three transitions from the 7^- isomer decay are present, herewith locating unambiguously both gating γ rays directly above the latter state. Prompt coincidence matrices constructed from the PPD cubes with suitable gates on delayed transitions were analyzed to develop the ^{118}Sn level scheme above the two isomers: The result is presented in Fig. 4. The energies and intensities of the new transitions are given in Table I together with their placement in the level scheme and the associated spin-parity assignments.

Apart from the 1426-keV transition, for which no evidence was found in the present data, the level scheme *above* the 10^+ isomer is essentially identical to that established by Fotiades *et al.* [10], but with more accurate transition and level energies. The observed transition intensities match well with those reported in Ref. [10], pointing to a similar population of states in fragments produced through fusion-fission processes with significantly different projectile-target combinations. The group of four levels located above the 7^- isomer that bypasses the 10^+ state was established for the first time in the present work. With the exception of the weak 541-keV branch, possibly depopulating the 3593-keV level to the 3052-keV

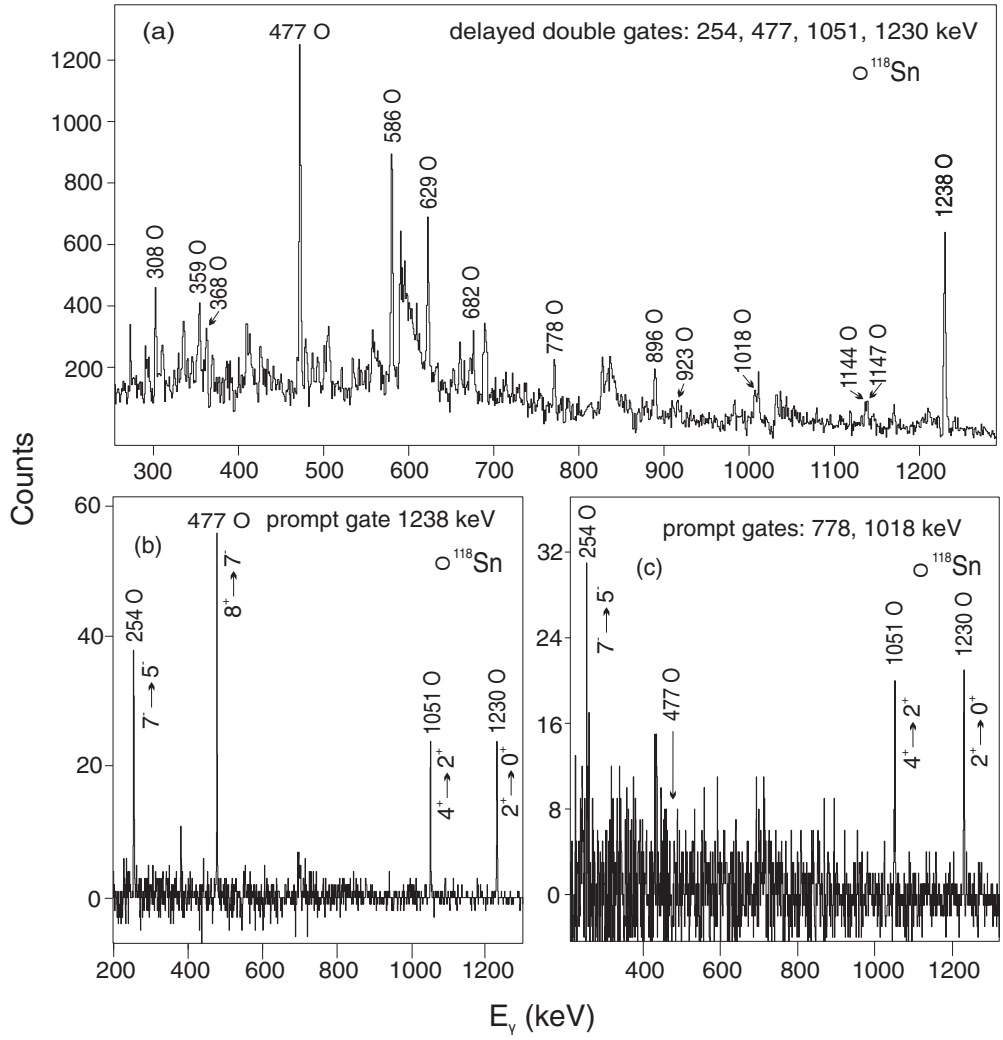

FIG. 3. Coincidence spectra in ^{118}Sn used to identify and place new transitions with respect to the 10^+ and 7^- isomers. Spectrum (a) was obtained with double-delayed-coincidence gates placed on all pairs among the 254-, 477-, 1051-, and 1230-keV γ rays. It shows all the prompt transitions preceding in time both isomers. The prompt gates indicated in the delayed spectra (b) and (c) represent branches feeding into the 10^+ and 7^- isomers, respectively (see text). γ rays identified with ^{118}Sn are labeled with open circles; other unmarked lines are arising from cross-coincidence relationships and from the (n,n') background.

8^+ state, no connection to any other known level could be traced in the data. Whereas negative parity is likely for these four states, the observed γ branching out of the 3593-keV level favors 8^- and 9^- tentative assignments to the 3352- and 3593-keV levels, respectively. For states located above the 10^+ isomer, considerations based on systematics (see Sec. IV) and on their clear yrast status allow one to propose the tentative assignments given in Fig. 4.

The $I^\pi = (12^+)$ assignment to the 4346-keV level had already been suggested by Fotiades *et al.* [10]. It is strongly supported by the distinct yrast location of the state and the fact that the excitation energy fits well within the systematics of the 12^+ states in even Sn isotopes. The 4932- and 5561-keV levels are also strongly populated in the yrast sequence and the systematics favors respective (13^-) and (15^-) assignments to these two states. It should be noted that, in principle, a (14^+) spin parity cannot be excluded for either state. However, an excitation energy of 4932 keV would be too low for a 14^+ state, according to the available systematics. With the relatively high population intensity of the 5561-keV level, the absence of an $E2$ branch to the (12^+) state in competition with the 628.5-keV decay to the (13^-) level makes a (14^+) assignment to this state unlikely as well. One of the relatively weakly populated levels at 5614 or 5855 keV is a possible candidate for such a (14^+) assignment. In any case, the observed γ-decay pattern sets an $I = 18$ upper limit for the spin of the highest-energy state observed at 6648 keV.

B. ^{120}Sn

As stated in Sec. II, the long 6.3- and 11.8-μs half-lives of the 10^+ and 7^- isomers in ^{120}Sn made the unambiguous identification of higher-lying transitions through straightforward delayed coincidence relationships difficult. Therefore, the analysis was started in this instance from the inspection of cross-coincidence spectra obtained by placing gates on

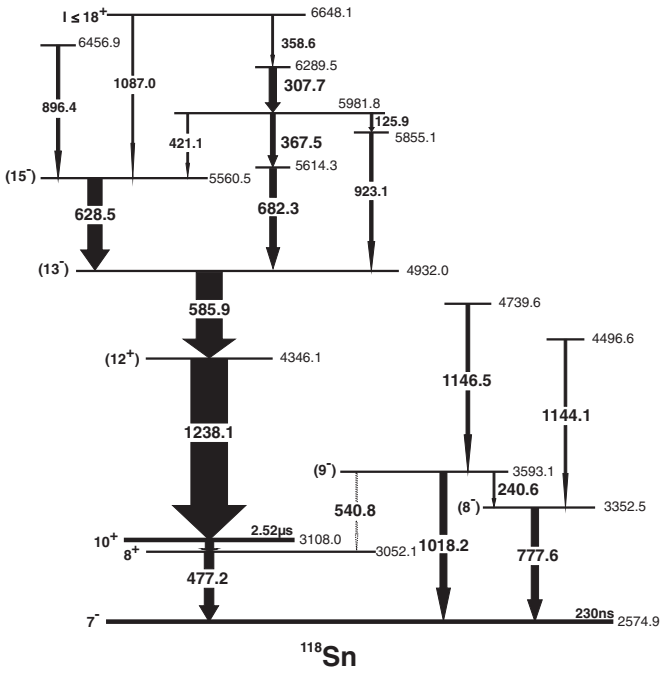

FIG. 4. The ^{118}Sn level scheme established in the present study. The arrow widths reflect the observed transition intensities. The spin-parity assignments are discussed in the text.

intense γ rays from the complementary fission fragments. This technique is discussed at some length in this instance as an example which also applies to the heavier ^{122,124}Sn cases.

Figure 5(a) is the sum of all coincidence spectra obtained from the PPP cube in the ^{48}Ca + ^{238}U data with double gates placed on the ground-state band transitions in Sm isotopes within the $A = 146$–154 mass range. In Fig. 5(b), a similar summed spectrum is presented with double gates placed on the strongest lines in Te isotopes with $A = 121$–127, as these are the complementary fragments to the Sn isotopes of interest in the ^{48}Ca + ^{208}Pb data. The energy range displayed in both figures covers the region where the most intense yrast transitions are expected in the level structures above the seniority-2 or -3 isomers in even and odd Sn isotopes, respectively. In spite of the inherent complexity of these spectra, the observed lines can be sorted out by associating them with different Sn isotopes, and this provided the starting point for the final identification, which was verified by subsequently establishing detailed level schemes for each isotope. The broad isotopic distribution of Sm and Te fragments did not allow conclusions to be drawn on the identification issue from the yields observed for individual complementary isotopes, but the variation of the intensity of observed Sn lines coincident with Sm and Te isotopes divided into lower and higher mass ranges provided good guidance toward isotopic assignments. Less complex spectra were obtained by exploiting the presence of isomeric states, which were subsequently established in the higher-lying level structures of all even Sn isotopes with mass $A > 118$. Examples are displayed in Figs. 6(a) and 6(b), where similar Sm and Te prompt double gates were selected from the respective PPD cubes to observe delayed transitions in Sn isotopes. The prompt 1238-keV line from the ^{118}Sn

TABLE I. List of the levels identified in ^{118}Sn with their respective spin-parity assignments. The last two columns list energies and relative intensities of the depopulating transitions as determined in the present study. The intensities have been normalized to that of the 1238-keV line, defined as 100 units.

E_{level} (keV)	I^{π}	E_{γ} (keV)	I_{γ}
2574.9	7^{-}		
3052.1	8^{+}		
3108.0	10^{+}		
3352.5	(8^{-})	777.6(1)	20(2)
3593.1	(9^{-})	240.6(3)	5(2)
		540.8(6)	$\leqslant$2
		1018.2(2)	19(2)
4346.1	(12^{+})	1238.1(1)	100
4496.6		1144.1(3)	7(2)
4739.6		1146.5(3)	10(2)
4932.0	(13^{-})	585.9(1)	71(4)
5560.5	(15^{-})	628.5(2)	39(4)
5614.3		682.3(2)	18(2)
5855.1		923.1(3)	9(2)
5981.8		125.9(3)	7(2)
		367.5(2)	13(2)
		421.1(5)	5(3)
6289.5		307.7(1)	20(2)
6456.9		896.4(3)	9(3)
6648.1		358.6(3)	5(2)
		1087.0(10)	5(3)

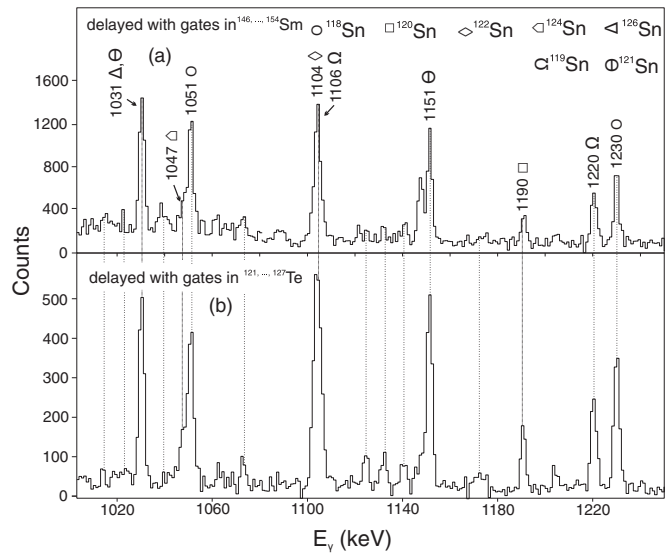

FIG. 5. High-energy parts of the cross-coincidence spectra obtained with gates placed on transitions emitted from fission fragments complementary to the Sn isotopes. The ground-state band transitions in Sm isotopes in the mass range $A = 146$–154 (a) and known transitions in Te isotopes with $A = 121$–127 (b) were selected in the ^{48}Ca + ^{238}U and ^{48}Ca + ^{208}Pb data, respectively. The main yrast transitions appearing in this energy range, associated with specific Sn isotopes, are labeled by symbols as indicated in the figure and described in the text.

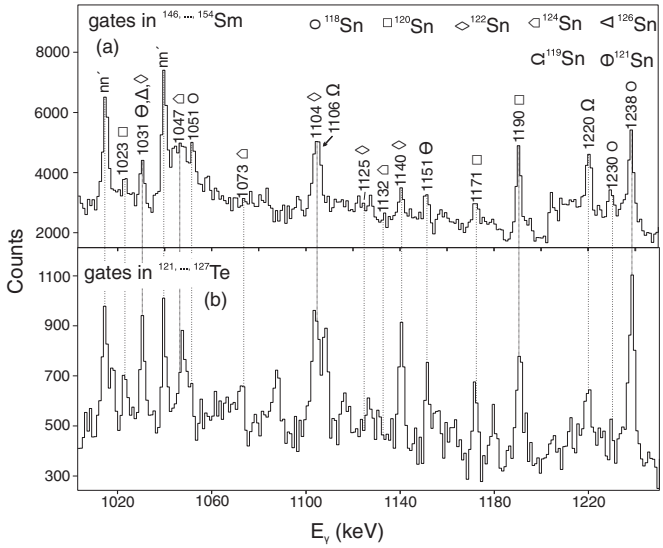

FIG. 6. Same as Fig. 5, but displaying transitions in Sn isotopes which are delayed in time with respect to the same gating, prompt transitions in the complementary fission fragments. These spectra enabled the identification of higher-lying isomers in the even-Sn isotopes (see text for details).

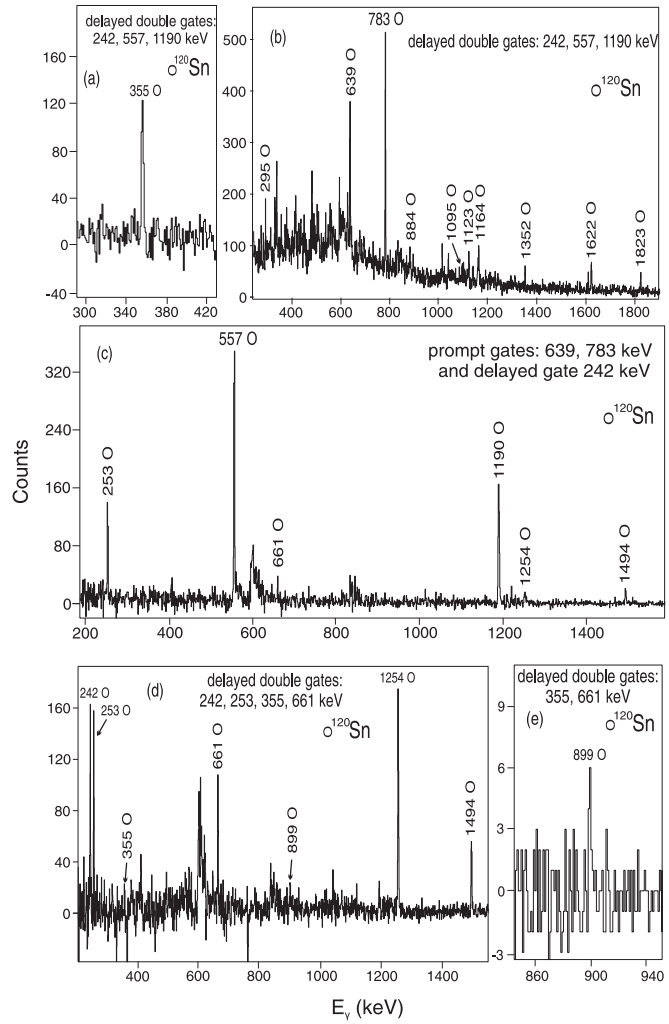

FIG. 7. Crucial coincidence spectra used to construct the ^{120}Sn level scheme. The complex selection of prompt and delayed gates is indicated in the corresponding panels. All panels provide delayed spectra, with the exception of panel (b), where prompt γ rays are shown. The detailed description of the gating conditions and of the conclusions drawn from the observed spectra can be found in the text.

isotope, which has no isomer above the 10^+ state, is seen clearly in the spectra of Figs. 5(a) and 5(b) but, as expected, is notably absent in the delayed spectra of Figs. 6(a) and 6(b). However, the 1190-, 1104-, and 1047-keV lines previously recognized as candidates for the isotopic identification are present in the delayed spectra of Fig. 6, and the inspection of the lower-energy parts of these spectra confirmed the presence of two additional delayed transitions which were found to be in prompt coincidence with each of the above-mentioned high-energy γ rays. These cross-coincidence results led to the conclusion that the observed families of three delayed transitions, i.e., the (242-557-1190-), (243-610-1104-), and (229-620-1047-) keV sequences, represent decays of high-spin isomers with most likely assignments to ^{120}Sn, ^{122}Sn, and ^{124}Sn, respectively.

In this way, the 1190-keV transition coincident with the strong 557- and 242-keV delayed γ rays was associated with a new ^{120}Sn isomer. The delayed spectrum obtained from the ddD cubes with double gates placed on all combinations of the prompt 242-, 557-, and 1190-keV lines confirmed this assignment. Indeed, this spectrum shows the expected 355-keV line [see Fig. 7(a)] corresponding to the $8^+ \rightarrow 7^-$ transition from the decay of the 6.3-μs isomer in ^{120}Sn; unlike in the case of ^{118}Sn above, however, the three γ rays following the decay of the 7^- state itself could not be observed owing to the long 11.8-μs half-life. This establishes the excitation energy of the new isomer as 4892 keV, with a dominant 242-, 557-, and 1190-keV decay cascade to the 10^+, 6.3-μs level. The half-life of this new isomer was determined to be 30(3) ns and, in the subsequent analysis, delayed-coincidence relationships with appropriate timing conditions clarified further features of the high-spin level scheme. Delayed double gates on the 242-, 557-, and 1190-keV lines selected the spectrum of prompt transitions preceding in time the isomer [Fig. 7(b)].

All the γ rays indicated by their energies are associated with the higher-lying levels in ^{120}Sn and were placed in the level scheme of Fig. 8. The latter scheme was constructed with the prompt γ-γ matrix preselected from the PPD cubes with delayed gates on transitions involved in the 30-ns isomer decay. Subsequently, the selection of the two most intense, higher-lying prompt transitions at 639 and 783 keV served to produce from the PDD cube the delayed-coincidence matrix used to search for other branches in the 30-ns isomer decay. The spectrum obtained from this matrix with the gate on the 242-keV isomeric transition is displayed in Fig. 7(c). Apart from the intense 557- and 1190-keV γ rays, it also indicates the presence of weaker 253-, 661-, 1254-, and 1494-keV lines associated with other decay branches from the isomer. The analysis of delayed γ-γ-γ coincidences within the time range appropriate for the 30-ns half-life firmly established this part of the decay scheme (Fig. 8). The combined double gates

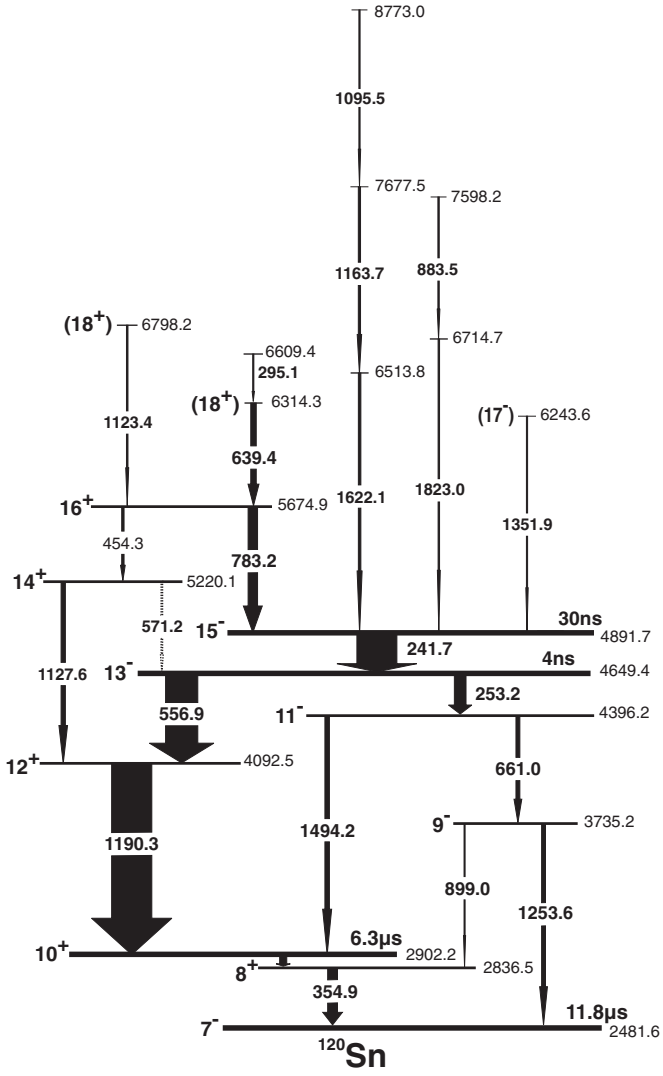

FIG. 8. The ^{120}Sn level scheme established in the present study with the convention on transition intensities adopted in Fig. 4. The spin-parity assignments are discussed in the text.

placed on the four transitions indicated in Fig. 7(d) provided the spectrum where transitions from this much weaker decay branch are enhanced. Specifically, the presence of weak 355- and 899-keV transitions is consistent with the connection of this decay branch toward the 2837-keV, 8^+ state. Indeed, the double gate placed on the 355- and 661-keV transitions confirmed the existence of the 899-keV connecting branch as displayed in Fig. 7(e). Finally, the analysis of prompt, in-beam γ-γ-γ coincidence events revealed the presence of 1128- and 454-keV transitions connecting the well-established 5675-keV level with the most intense 1190-keV yrast transition.

Table II lists the levels, transition energies, and intensities observed in ^{120}Sn. The scheme of Fig. 8 confirms the four transitions of Ref. [10] and the states proposed by Astier *et al.* [11]. However, the present results include an important additional branch in the decay of the 30-ns isomer as well as a significantly extended structure above this long-lived state. Whereas the lifetime determinations are discussed in a separate section below, it should be pointed out that a 4(1)-ns half-life was determined here for the 4649-keV state populated in the 30-ns isomer decay.

TABLE II. Same as Table I, but for ^{120}Sn. The intensities of γ rays are normalized to that of the 1190-keV line.

E_{level} (keV)	I^π	E_γ (keV)	I_γ
2481.6	7^-		
2836.5	8^+		
2902.2	10^+		
3735.2	9^-	899.0(6)	1.0(4)
		1253.6(2)	12(2)
4092.5	12^+	1190.3(1)	100
4396.2	11^-	661.0(2)	10(2)
		1494.2(2)	12(2)
4649.4	13^-	253.2(2)	30(3)
		556.9(1)	83(5)
4891.7	15^-	241.7(1)	103(5)
5220.1	14^+	571.2(9)	$\leqslant 3$
		1127.6(3)	11(2)
5674.9	16^+	454.3(3)	6(1)
		783.2(3)	23(2)
6243.6	(17^-)	1351.9(4)	3(1)
6314.3	(18^+)	639.4(4)	14(2)
6513.8		1622.1(3)	6(2)
6609.4		295.1(4)	3(1)
6714.7		1823.0(4)	4(1)
6798.2	(18^+)	1123.4(4)	4(1)
7598.2		883.5(4)	3(1)
7677.5		1163.7(4)	6(2)
8773.0		1095.5(5)	3(1)

Apart from the limited angular-correlation results reported by Astier *et al.* [11], no other direct experimental determination of transition multipolarities is available. Nevertheless, firm spin-parity assignments are proposed for states up to the 16^+ level at 5675 keV on the basis of the observed decay sequences while also taking into account well founded expectations, systematics, and yrast population arguments. Whereas this approach is outlined below in the case of ^{120}Sn, similar considerations led to firm spin-parity assignments for other isotopes as well. Confidence in the assignments is supported further by the overall consistency observed in the full sequence of even Sn isotopes.

Shell-model expectations supported by calculations presented in the discussion section below, as well as considerations based on systematics in the heavier even Sn isotopes, indicates a 15^- assignment to the 30-ns isomer. Any higher-spin value is excluded by the presence of the strong decay sequence of four 242-, 253-, 661-, and 1254-keV transitions connecting it with the 7^- isomer. The measured half-lives and the limits on the lifetimes of the states involved in this sequence (<3 ns) exclude an $M2$ or higher-order multipolarity for any of these four transitions. On the other hand, a lower spin value (e.g., $I = 14$) for the isomer is inconsistent as well with the various observed decay branches and with the measured lifetimes. Consequently, these four lines must all be of $E2$ multipolarity. The measured half-lives are also consistent with

the $E2$ assignments to the 242- and 253-keV γ rays and, thus, the 3735-, 4396-, and 4649- keV levels are uniquely assigned as 9^-, 11^-, and 13^- states, which are also depopulated by the observed 899-, 1494-, and 557-keV $E1$ branches to the 8^+, 10^+, and 12^+ yrast states. The strong, yrast population of the 5675-keV level favors a 16^+ assignment, as this is consistent with the observed decay and favors the 14^+ spin and parity proposed for the 5220-keV state depopulated by an 1128-keV (apparent $E2$) transition to the lowest 12^+ level. The observation of the 1352-, 1123-, and 639-keV transitions as sharp lines, in the absence of strong feeding from higher-lying levels, suggests few-ps lifetimes for the corresponding states. This, in turn, favors $E2$ assignments and the 6244-, 6798-, and 6314-keV levels are tentatively assigned as 17^-, 18^+, and 18^+, respectively. The established feeding from higher-lying levels prevents any conclusion for the other observed states and their spins and parities remain unassigned.

C. ^{122}Sn

The cross-coincidence analysis technique discussed above for ^{120}Sn also provided the initial identification of the 4721-keV isomeric state in ^{122}Sn together with its main decay path through the 243-, 610-, and 1104-keV transitions toward the long-lived 10^+ level. The measured half-life of 134(12) ns was well suited to impose timing conditions for the selection of the delayed-coincidence events that were instrumental in identifying the many γ rays and in delineating the various decay paths in ^{122}Sn. The complete level scheme of higher-seniority ($\nu > 2$) states is displayed in Fig. 9. It was established in a manner similar to that described above for the ^{120}Sn isotope. Here as well, the sequence of transitions feeding the 7^- long-lived state verified the ^{122}Sn isotopic assignment, in agreement with the earlier identifications of Refs. [10,11]. The part of the level scheme involving the most intense transitions (Fig. 9) confirms the findings of Ref. [11], but the present study is more detailed and includes many previously unobserved transitions and features. The complete list of levels with the γ-ray energies and intensities determined in the present work can be found in Table III. The most important new results are documented through the spectra selected in Fig. 10. In the top panel [Fig. 10(a)], the γ rays preceding in time the 134-ns isomer are displayed. This spectrum was obtained from all the available PDD data with delayed double gates on the strong 243-, 610-, and 1104-keV transitions located below the isomer. Every marked line was placed in the level scheme of Fig. 9 based on the analysis of a γ-γ coincidence matrix selected from the PPD cubes by placing delayed single gates on the same three transitions. The branching in the isomeric decay (see Fig. 9) is illustrated by the spectrum in Fig. 10(b) obtained from the PDD cubes by placing prompt gates on any of the three most intense γ rays above the isomer together with a delayed gate placed on the 243-keV isomeric transition. The main branch competing with the strong 610-keV transition is represented by the 265-keV line, which has a relative intensity similar to the analogous branch in ^{120}Sn. It turned out that the 4479-keV level, where this branching in the decay out of the 134-ns isomer occurs, also has a fairly long half-life of 40(3) ns; this is demonstrated in Fig. 10(c) by showing

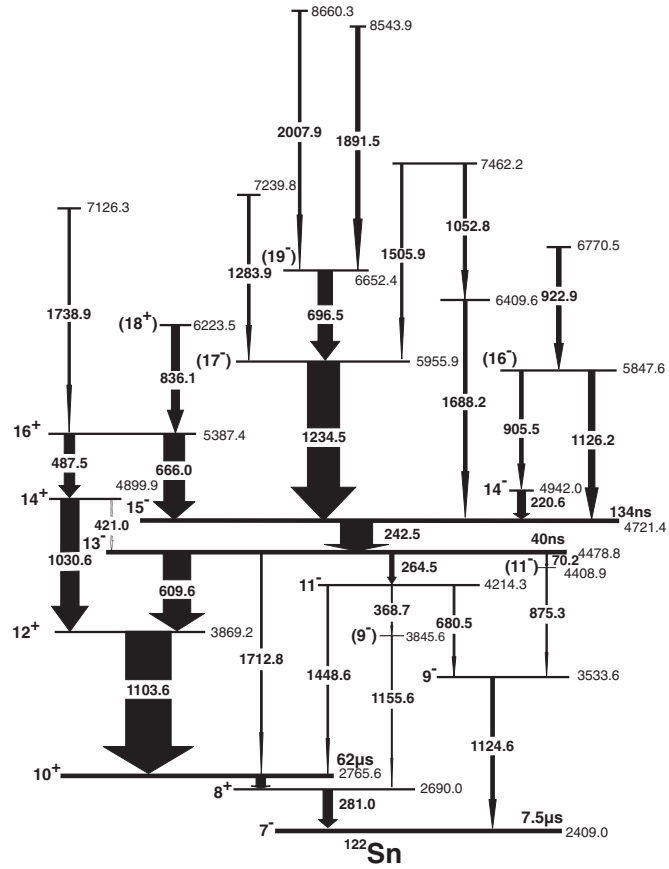

FIG. 9. The ^{122}Sn level scheme established in the present study with the convention on transition intensities adopted in Fig. 4. The spin-parity assignments are discussed in the text.

that the delayed 243-keV transition precedes in time the 610- and 1104-keV transitions which are delayed even further. Figure 10(d) presents a delayed spectrum from the DDD cube with a double gate placed on the 243- and 265-keV lines. Apart from the main decay branches of 681 and 1125 keV along the path to the 7^- isomer and the 1449-keV link to the 10^+ long-lived state, the spectrum points to the presence of a much weaker 369-1156-keV sequence linking the 40-ns isomer to the 8^+ yrast state. This branch was confirmed by the coincidence relationships between these three γ rays. Finally, Fig. 10(e) provides a spectrum obtained with a delayed double gate placed on the 1125- and 243-keV transitions to illustrate the 70-875-keV decay path from the 4479-keV isomer. The 40-ns half-life favors the placement of the low-energy 70-keV γ ray as one of the isomeric transitions and the observed intensity, albeit with large uncertainty, is compatible with the high electron conversion inherent to an $E2$ transition. Moreover, a dedicated search carried out to observe yet another possible branch connecting the 4479-keV level directly to the 10^+ isomer established the high-energy, 1713-keV transition, which is assigned an $E3$ multipolarity, based on the 13^- spin-parity assignment to the 40-ns isomer.

Spin and parity quantum numbers are assigned to the 134-ns, 15^- isomeric state and to the lower-lying levels populated in its decay on the basis of considerations similar

TABLE III. Same as Table I, but for ^{122}Sn. To normalize the relative intensities of γ transitions below the 15^- isomer, the 100 units of intensity were defined from the yield of the 243-keV isomeric transition. Intensities of prompt lines above and bypassing the isomer and marked with a * symbol were normalized separately with 100 units attributed to the most intense, 1235-keV transition.

E_{level} (keV)	I^π	E_γ (keV)	I_γ
2409.0	7^-		
2690.0	8^+		
2765.6	10^+		
3533.6	9^-	1124.6(2)	11(2)
3845.6	(9^-)	1155.6(4)	2(1)
3869.2	12^+	1103.6(1)	139(6)[a]
4214.3	11^-	368.7(4)	2(1)
		680.5(2)	6(1)
		1448.6(2)	5(1)
4408.9	(11^-)	875.3(3)	4(1)
4478.8	13^-	70.2(5)	0.60(13)[b]
		264.5(2)	13(2)
		609.6(1)	83(4)
		1712.8(5)	3(1)
4721.4	15^-	242.5(1)	100
4899.9	14^+	421.0(9)	$\leqslant 3$
		1030.6(2)	56(4)*
4942.0	14^-	220.6(3)	25(3)*
5387.4	16^+	487.5(2)	32(2)*
		666.0(2)	65(3)*
5847.6	(16^-)	905.5(3)	11(2)*
		1126.2(2)	20(3)*
5955.9	(17^-)	1234.5(1)	100*
6223.5	(18^+)	836.1(3)	25(2)*
6409.6		1688.2(5)	11(3)*
6652.4	(19^-)	696.5(3)	45(3)*
6770.5		922.9(3)	14(2)*
7126.3		1738.9(5)	7(2)*
7239.8		1283.9(4)	8(2)*
7462.2		1052.8(4)	10(3)*
		1505.9(5)	7(2)*
8543.9		1891.5(4)	13(2)*
8660.3		2007.9(5)	8(2)*

[a]The summed intensity of prompt and delayed feeding is given.
[b]The very weak 70-keV γ ray was observed, but its intensity was calculated assuming an $E2$ electron conversion coefficient [20] and a total transition intensity equal to that of the 875-keV transition.

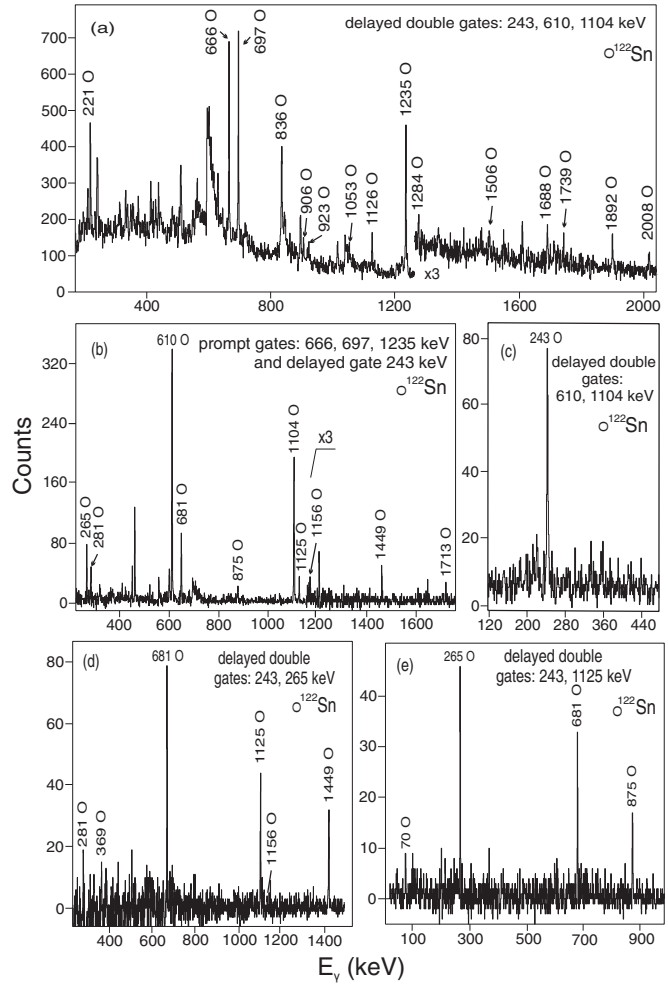

FIG. 10. Crucial coincidence spectra used to construct the ^{122}Sn level scheme. The gating conditions are indicated in each panel and are explained in the text. Spectrum (a) shows prompt transitions above the 15^- isomer, delayed spectra (b) and (c) document the existence of the 13^- isomer, and delayed spectra (d) and (e) illustrate branches in the isomeric decay.

to those discussed in the case of ^{120}Sn. The 40-ns half-life of the 4479-keV isomer, assigned as the 13^- state, enables one to observe four decay branches of which the 610-keV $E1$ and 1713-keV $E3$ transitions populate directly the respective 3869-keV 12^+ and 2766-keV 10^+ levels, while the other two feed the two 11^- states at 4214 and 4409 keV through the 265- and 70-keV $E2$ transitions. The latter two levels, in turn, populate the two 9^- states at 3534 and 3846 keV. These assignments are the only ones that are fully compatible with the decay patterns of the observed levels and with the measured lifetimes. Moreover, they are supported further by analogies with the level structures seen in other even Sn isotopes, and they are also consistent with the results of shell-model calculations presented in the discussion section below. The analysis of triple prompt coincidences revealed the presence of the intense 1031-488-keV sequence above the 12^+ 3869-keV yrast level which provides a deexcitation from the 5387-keV state bypassing the 15^- isomer. Considerations based on the analogy with the ^{120}Sn scheme and on the definite yrast nature of this strongly populated 5387-keV level lead to the proposed 16^+ assignment which, in turn, requires the 14^+ one to the intermediate level at 4900 keV. The observed population intensities also indicate an yrast character for the 5956-, 6224-, and 6652-keV states and these are given tentative 17^-, 18^+, and 19^- respective assignments as a result. However, the observed intensity of the low-energy 221-keV transition placed directly above the 15^- isomer most likely points to a deexcitation from a nonyrast level. Such a state was not observed in ^{120}Sn but, as shown later, similar nonyrast levels are seen in heavier Sn isotopes. The 14^- spin parity assigned to this state is expected for a level based on the same configuration as the

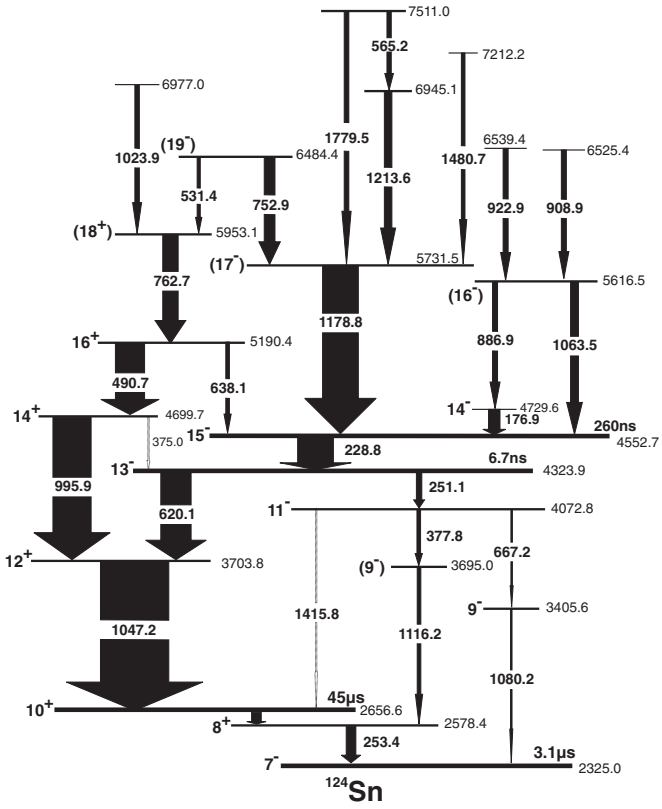

FIG. 11. The ^{124}Sn level scheme established in the present study with the convention on transition intensities adopted in Fig. 4. The spin-parity assignments are discussed in the text.

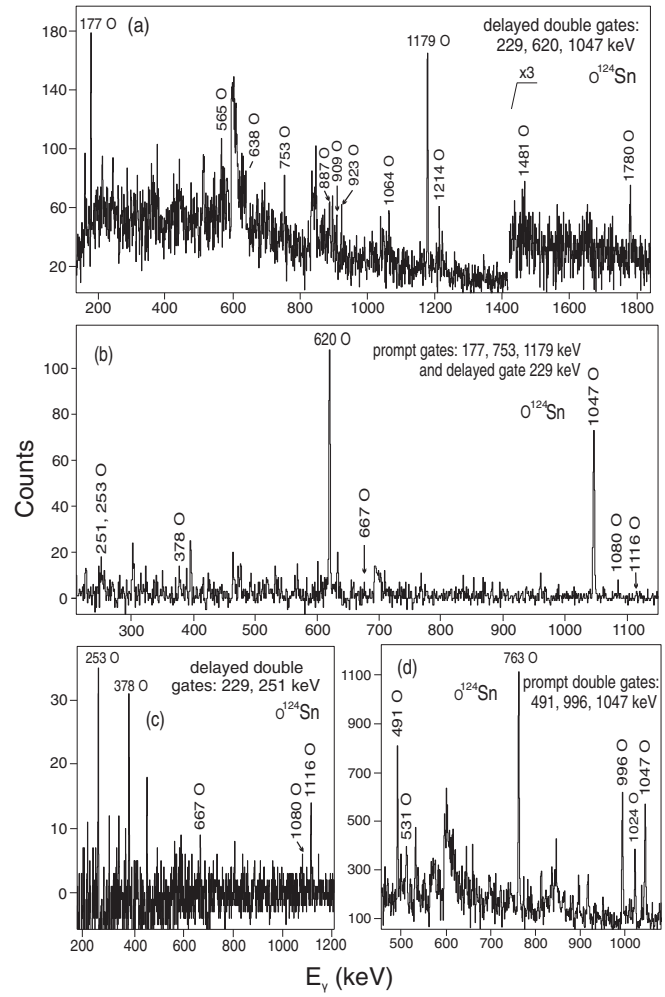

FIG. 12. Examples of coincidence spectra used to construct the ^{124}Sn level scheme. The gating conditions are indicated in each panel and are explained in the text. Spectrum (a) displays prompt transitions above the 15^- isomer, delayed spectra (b) and (c) document the γ branching in the 13^- isomeric decay, and a prompt spectrum (d) provides evidence for the sequence of transitions bypassing the 15^- isomer.

15^- isomer, but with four neutrons coupled to a spin lower by one unit. The shell-model calculations indeed predict a 14^- state at this excitation energy (see below). Furthermore, the absence of a competing $M1$ transition to the lower-lying 13^- level is not surprising in view of the configurations involved. The shell-model calculation also indicated the 5848-keV state as a good candidate for the 16^- spin-parity assignment; the observed $E2$ transition to the 14^- level and a more intense $M1$ decay to the 15^- isomer support such assignment. No spin-parity quantum numbers are proposed for a number of other states in the level scheme (Fig. 9), although the observed decay features combined with considerations based on feeding patterns could result in preferred assignments in some instances.

D. ^{124}Sn

With an identification procedure similar to that discussed above for ^{120,122}Sn, the 229-620-1047-keV cascade could be established as the main decay path from the 15^-, 260(30)-ns isomer in ^{124}Sn and this sequence also provided first access to the higher-seniority states located above the long-lived 10^+ isomer. In the present study, this part of the level scheme which involves the most intense transitions is fully consistent with the first identification in Ref. [10] and the more extensive results of Ref. [11]. Nevertheless, the present ^{124}Sn level scheme in Fig. 11 is more complete: Apart from new pathways associated with the deexcitation of the 15^- isomer, it also involves a well-developed structure of high-energy levels not observed earlier. The spectra presented in the various panels of Fig. 12 were selected to specifically document these new results.

The spectrum of Fig. 12(a) served to identify all the transitions preceding in time the 15^- isomeric decay. As in the ^{120}Sn case, it was obtained from all the available data by placing in the PDD cubes delayed double gates on the three strong γ rays mentioned above. The lines of interest are marked in Fig. 12(a) by their respective energies. All of these were also placed in the level scheme (Fig. 11) on the basis of coincidence relationships established from the prompt γ-γ matrix obtained from the PPD cubes by requiring a delayed coincidence with transitions following the isomeric decay. It can be noticed that the statistics and the general quality of the spectrum in Fig. 12(a) are not as good as the corresponding data for both ^{120}Sn and ^{122}Sn. This is a

TABLE IV. Same as Table I, but for ^{124}Sn. The normalization of the γ-ray intensities is similar to that used in Table III, but with the 100 units attributed to the 229- and 1179-keV transitions for delayed and prompt transitions, respectively.

E_{level} (keV)	I^{π}	E_{γ} (keV)	I_{γ}
2325.0	7^-		
2578.4	8^+		
2656.6	10^+		
3405.6	9^-	1080.2(3)	4(1)
3695.0	(9^-)	1116.2(2)	10(2)
3703.8	12^+	1047.2(1)	192(6)[a]
4072.8	11^-	377.8(2)	10(2)
		667.2(3)	4(1)
		1415.8(9)	$\leqslant$2
4323.9	13^-	251.1(2)	15(2)
		620.1(1)	85(4)
4552.7	15^-	228.8(1)	100
4699.7	14^+	375.0(9)	$\leqslant$3
		995.9(2)	107(5)*
4729.6	14^-	176.9(2)	32(2)*
5190.4	16^+	490.7(2)	82(4)*
		638.1(3)	10(2)*
5616.5	(16^-)	886.9(3)	14(2)*
		1063.5(2)	22(3)*
5731.5	(17^-)	1178.8(1)	100*
5953.1	(18^+)	762.7(3)	43(3)
6484.4	(19^-)	531.4(2)	9(2)
		752.9(2)	30(3)*
6525.4		908.9(4)	14(3)*
6539.4		922.9(3)	14(2)*
6945.1		1213.6(3)	21(3)*
6977.0		1023.9(2)	12(2)
7212.2		1480.7(3)	10(2)*
7511.0		565.2(5)	12(3)*
		1779.5(3)	13(3)*

[a]The summed intensity of prompt and delayed feeding is given.

consequence, on the one hand, of the lower ^{124}Sn production yield and, on the other, of the lower relative population of the 15^- isomer attributable to the fact that more than 50% of the yrast population proceeds via positive-parity states bypassing the long-lived state. Table IV lists all the levels, transition energies, and intensities established in the present work for ^{124}Sn.

From Fig. 11 and Table IV one can also see that the decay paths connecting the 15^- isomer with the 8^+ and 7^- seniority-2 states are weaker than the corresponding branches in ^{120}Sn. This can be readily inferred from the spectrum of Fig. 12(b) obtained from the PDD cubes with prompt gates placed on any of the intense γ rays above the isomer together with a delayed gate on the 229-keV isomeric transition. The small intensity of the 251-keV line compared to the 620-keV γ ray representing the main decay path illustrates this feature. In spite of the low intensity, this spectrum also indicates the presence of the 378- and 1116-keV transitions from the branch to the 2578-keV 8^+ state. The spectrum obtained from the DDD cube with double gate on the 229- and 251-keV transitions [Fig. 12(c)] provides further evidence for this branch with the 253-keV, $8^+ \rightarrow 7^-$ transition matching the high intensity of the 378- and 1116-keV lines. In this spectrum, weaker 667- and 1080-keV transitions are present as well; from a detailed coincidence analysis, these have been associated with a decay branch to the 7^-, 2325-keV isomer. The observed decay pattern firmly confirms the identification of the 15^- isomer and, in analogy with the observations in ^{120,122}Sn, a 6.7(9)-ns half-life was determined for the 4324-keV, 13^- level. However, only tentative evidence was found for the 1416-keV, $11^- \rightarrow 10^+$ transition with the intensity limit indicated in Table IV. No trace of a 1667-keV, $13^- \rightarrow 10^+$ $E3$ transition was uncovered.

The combination of double gates placed on the 491-, 996-, and 1047-keV lines in the PPP cube produced the spectrum of Fig. 12(d) showing the sequence of transitions between the positive-parity states resembling closely those seen in the lighter Sn isotopes. As mentioned above, this large-intensity cascade mostly bypasses the isomer with only a weak, 638-keV line feeding the 15^- long-lived state from the 5190-keV level. In addition to the three strong gating transitions, Fig. 12(d) also displays the 763- and 1024-keV γ rays extending the sequence to higher-lying states as well as the 531-keV line connecting it to the 6484-keV level established independently through the analysis of the structure built on the 15^- isomer itself.

Based on considerations similar to those presented for ^{120}Sn and ^{122}Sn, a spin and parity of 15^- is assigned to the 4553-keV isomer and 13^- to the 4324-keV, 6.7-ns state. Subsequently, the lower-lying 4073-keV level is assigned as the 11^- state. The latter is, in turn, depopulated via two intermediate 9^- levels at 3695- and 3406-keV to the 8^+ and 7^- seniority-2 states, respectively. In analogy to lighter Sn isotopes, the most intense yrast sequence above the 12^+, 3704-keV state establishes the 14^+ level at 4700 keV and the 16^+ yrast state at 5190 keV. In agreement with the trend observed in the depopulation of the corresponding 16^+ level in both ^{120}Sn and ^{122}Sn, the 638-keV $E1$ decay to the 15^- isomer is much weaker than the 491-keV $E2$ link to the 14^+ state. Considerations about yrast population and analogies with the ^{120}Sn and ^{122}Sn level schemes enabled the 14^- assignment to the 4730-keV state and yielded tentative, but likely 16^-, 17^-, 18^+, and 19^- assignments to the 5617-, 5732-, 5953-, and 6484-keV levels. In general, similar considerations could also apply to some of the other states observed and tentative spin-parity assignments could be suggested. However, the assignments proposed here have been restricted to the clearest cases in view of the limited reliability of shell-model calculations for seniority $\nu = 6$ states.

E. ^{126}Sn

In the investigation of the ^{126}Sn isotope, which is produced with smaller yields, only the data from the ^{48}Ca + ^{238}U and ^{64}Ni + ^{238}U reactions were used to extract the information on higher-seniority levels listed in Table V. The initial cross-coincidence identification of the three delayed 181-, 571-, and 1031-keV transitions as candidates for the 15^- isomer decay in ^{126}Sn was confirmed by a dedicated sort where two delayed γ rays were required to be followed by a third, even more delayed one. The spectrum in Fig. 13(a) indicates that the

TABLE V. Same as Table I, but for ^{126}Sn. The normalization of the γ-ray intensities is similar to that used in Table III, but with the 100 units attributed to the 181- and 1150-keV transitions for delayed and prompt transitions, respectively.

E_{level} (keV)	I^{π}	E_{γ} (keV)	I_{γ}
2217.7	7^-		
2487.0	8^+		
2563.3	10^+		
3282.7	9^-	1065.0(3)	8(2)
3594.2	12^+	1030.9(1)	154(9)[a]
3924.7	11^-	642.2(2)	8(2)
		1361.6(3)	10(2)
4165.2	13^-	240.5(2)	18(2)
		571.0(1)	82(5)
4346.0	15^-	180.8(1)	100
4559.7	14^-	213.7(3)	19(2)*
4581.8	14^+	987.6(4)	72(5)*
5059.7	16^+	477.9(4)	45(4)*
		713.7	<3
5496.0	(17^-)	1150.0(1)	100*
5836.9	(18^+)	777.2(5)	22(2)
6257.5	(19^-)	761.5(2)	40(3)*
7322.7		1826.7(5)	8(2)*
8374.1		2116.6(6)	18(3)*

[a]The summed intensity of prompt and delayed feeding is given.

expected 269-keV, $8^+ \rightarrow 7^-$ transition in ^{126}Sn is delayed with respect to the three strong 181-, 571-, and 1031-keV lines

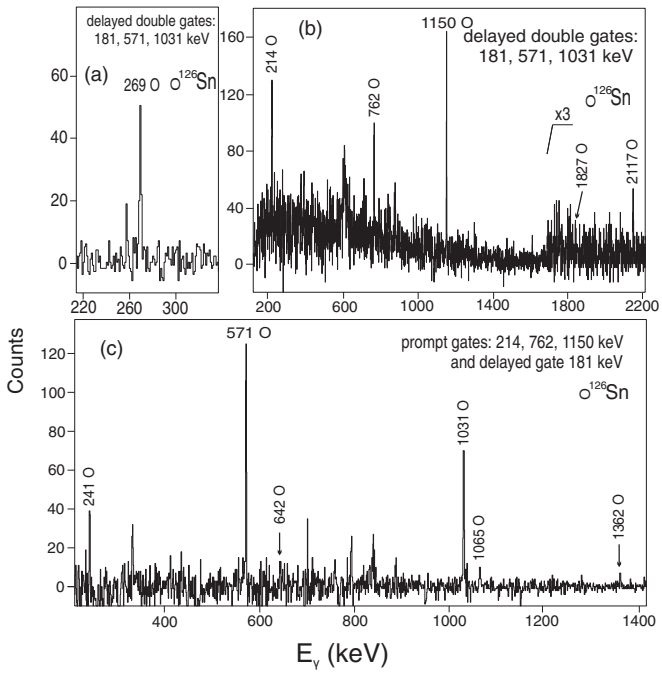

FIG. 13. Examples of coincidence spectra used to establish the ^{126}Sn level scheme. The gating conditions are indicated in each panel and are explained in the text. Spectrum (a) documents the identification of gated γ rays as preceding in time the 10^+ ^{126}Sn isomer, prompt (b) and delayed (c) spectra display transitions located above and below the 15^- isomer, respectively.

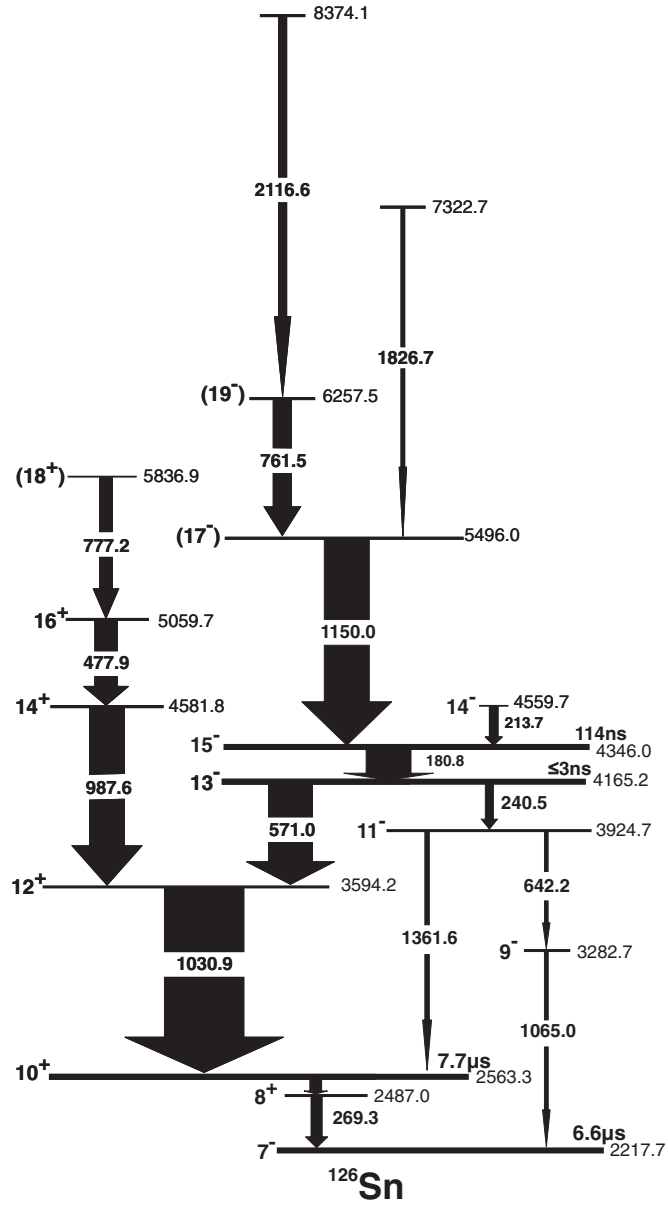

FIG. 14. The ^{126}Sn level scheme established in the present study with the convention on transition intensities adopted in Fig. 4. The spin-parity assignments are discussed in the text.

used as gates in the ddD cubes. This is in agreement with the findings of Ref. [11], although the half-life of the 15^- isomer determined here, $T_{1/2} = 114(12)$ ns, is significantly shorter than the 160(20)-ns published value. The present ^{126}Sn level scheme (Fig. 14) also includes transitions not reported earlier. The selection of delayed double gates (in the PDD cube) placed on three lines below the 15^- isomer (181, 571, 1031 keV) provided a clean identification of transitions above the isomer, as can be inferred from Fig. 13(b). Here, apart from the 762- and 1150-keV transitions reported in Ref. [11], the 214-, 1827-, and 2117-keV γ rays were identified and placed in the level scheme. The usual prompt γ-γ matrix selected by requiring the presence of one of the three strong delayed lines below the 15^- isomer served to verify the coincidence relationships

and establish a low-lying 4560-keV level depopulated by the 181-keV transition (in analogy with the 14^- states seen in the other Sn isotopes), as well as to place the 1827- and 2117-keV lines in the highest part of the level scheme. It should be noted that the observation of the 1827- and 2117-keV γ rays as discrete narrow lines, in the absence of low-energy transitions feeding the corresponding states, makes an $M1$ multipolarity unlikely. The spectrum of Fig. 13(c) obtained from the PDD cube with gates placed on one of the prompt γ rays above the 15^- isomer and on the 181-keV delayed isomeric transition indicates the presence of an additional decay path that had not been observed before. Along with the strong 571-1031-keV main decay branch, much weaker 241-, 642-, 1065-, and 1362-keV γ rays are seen which were uniquely placed in the level scheme of Fig. 14 based on the analysis of the DDD coincidence events.

As was the case in the other isotopes, the decay branches to the 7^- and 10^+ long-lived states observed here solidify the identification and the 15^- spin-parity assignment of the 4346-keV isomer in ^{126}Sn. In the same way, the levels at 3283, 3594, 3925, and 4165keV can be respectively assigned as the 9^-, 12^+, 11^-, and 13^- states with confidence. Prompted by the results on the lighter Sn isotopes, a search for a measurable lifetime for the 13^- level was carried out, resulting in a $T_{1/2} \leqslant 3$ ns limit. The analysis of prompt PPP coincidence events established the 4582-, 5060-, and 5837-keV levels with 14^+, 16^+, and tentative 18^+ respective assignments. This result matches the data of Ref. [11] and the assignments are based on the analogy with similar cascades in the other Sn isotopes. It should be noted that the more accurate transition energies of Table V are in some cases rather different from those quoted in Ref. [11]. Also, the decay branch from the 16^+ level to the 15^- isomer seen in ^{120,122,124}Sn could not be observed in ^{126}Sn. Finally, in the ^{126}Sn level scheme of Fig. 14, apart from the 14^- state discussed above, only the 5496- and 6258-keV levels above the 15^- isomer were tentatively given 17^- and 19^- assignments, given their prominent yrast feeding.

F. ^{128}Sn

The 15^- isomer in ^{128}Sn was identified by Pietri *et al.* [12] and their decay scheme was instrumental in confirming that this long-lived state was also produced in the present work. It is seen in reactions using a ^{238}U target and then only with small yields. Unfortunately, the small production cross sections did not allow for an expansion of the level scheme beyond that of Ref. [12]: No γ rays could be identified above the isomer and, as a result, the half-life of the 15^- level could not be checked through appropriate PDD or PPD cubes. For completeness, the confirmed decay sequences are displayed in Fig. 15.

TABLE VI. Same as Table I, but for ^{128}Sn. The intensities of γ rays are normalized to the 120-keV isomeric transition, defined as 100 units.

E_{level} (keV)	I^π	E_γ (keV)	I_γ
2091.5	7^-		
2412.7	8^+		
2492.0	10^+		
3146.6	9^-	1055.1(3)	36(4)
3554.0	12^+	1062.0(3)	64(6)
3771.9	11^-	625.3(3)	36(4)
3980.0	13^-	207.6(3)	36(4)
		426.0(2)	64(6)
4099.7	15^-	119.7(2)	100

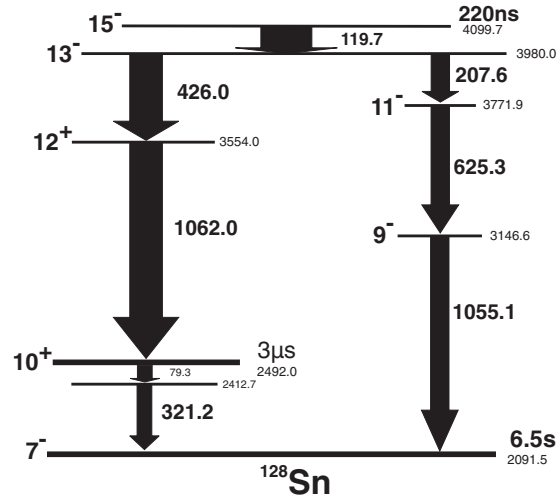

FIG. 15. The ^{128}Sn level scheme established in the present study with the convention on transition intensities adopted in Fig. 4. The spin-parity assignments are discussed in the text.

The measured transition energies are somewhat more precise than in Ref. [12]: They can be found in Table VI together with the measured intensities. The spin-parity assignments tentatively proposed in Ref. [12] are now supported by the noted analogy with the 15^- isomeric decays in the other Sn isotopes. However, any further extension of the ^{128}Sn level scheme will require a dedicated new experiment.

G. Half-life determinations

Half-lives were determined for the 15^- levels observed in the present work by fitting time distributions obtained with double coincidence gates placed on (1) the most intense prompt γ rays above each long-lived state, and (2) on the three delayed transitions in the most intense decay branch. In the case of ^{122}Sn, however, only the 243-keV, $15^- \rightarrow 13^-$ transition was used to avoid the interference by the half-life of the 13^- state. The latter $T_{1/2}$ value was shown to be significantly longer than in the other cases, where this effect could be neglected. In Fig. 16, these time distributions are compared with the results of the fits for the 15^- isomers observed in ^{120,122,124,126}Sn. In each case, the gating transitions are given in the various panels of the figure. The half-life values reported here agree well with those of Ref. [11] for ^{120}Sn and ^{124}Sn. Although the 146(15)-ns half-life determined in Ref. [11] for ^{122}Sn agrees within errors with the present 134(12)-ns value, the observed small difference was found to be associated with the presence of the 13^- isomer, which was taken into account only in the present analysis. However, the present 114(12)-ns half-life value for

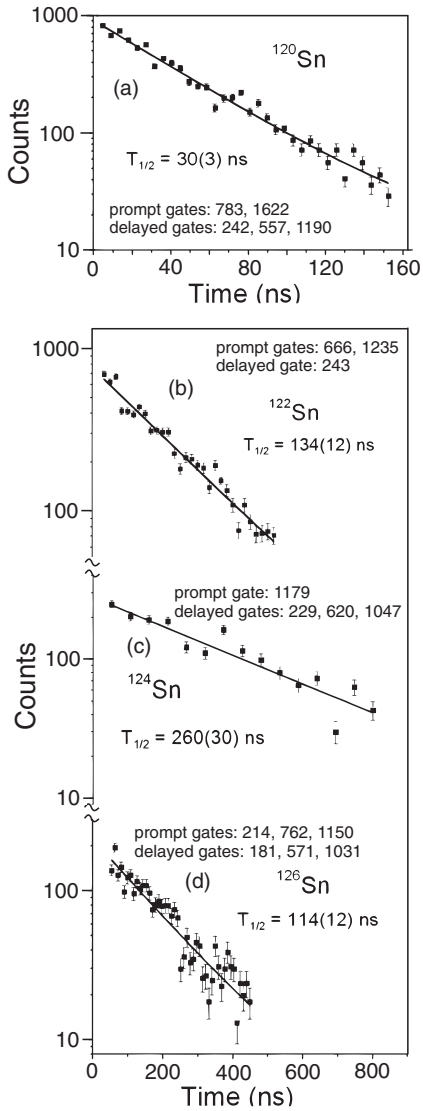

FIG. 16. γ-γ time distributions used to determine the half-lives of the 15^- isomers in ^{120}Sn (a), ^{122}Sn (b), ^{124}Sn (c), and ^{126}Sn (d). The time spectra were obtained by placing energy gates on the most intense prompt transitions above and delayed γ rays below the isomers as indicated in each panel (see text for details).

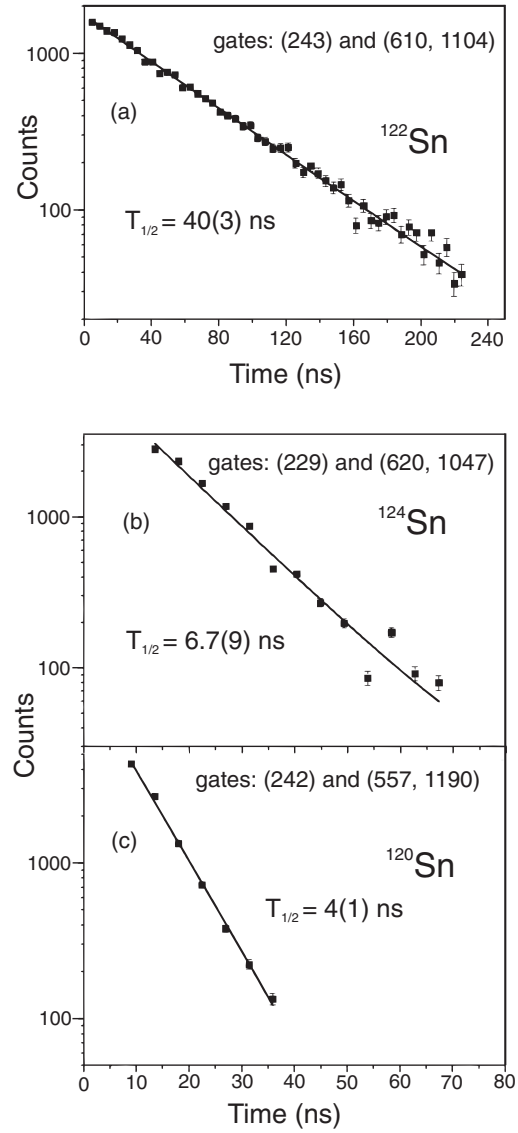

FIG. 17. γ-γ time distributions used to determine the half-lives of the 13^- isomers in ^{122}Sn (a), ^{124}Sn (b), and ^{120}Sn (c). The time spectra were obtained by placing gates on the $15^- \rightarrow 13^-$ transition known in each isotope and double gates on transitions of the corresponding $13^- \rightarrow 12^+ \rightarrow 10^+$ sequences (see text for details).

the 15^- isomer in ^{126}Sn is lower than the 160(20)-ns value quoted in Ref. [11] for unknown reasons.

As discussed in Sec. III C above, the observed half-life of 40(3) ns was instrumental in defining the 13^- state in ^{122}Sn as an isomer. This result initiated a timing analysis for the corresponding 13^- levels in the other even-Sn isotopes. Figure 17 displays time distributions obtained from the delayed events only, with gates placed in each case on the $15^- \rightarrow 13^-$ γ ray and on two transitions below the 13^- level. The gate selection and fitting results are indicated in each panel of Fig. 17 and half-lives of 40(3), 6.7(9), and 4(1) ns were determined for the 13^- states in ^{122}Sn, ^{124}Sn, and ^{120}Sn, respectively.

The measured half-lives and intensities of the observed γ-decay branches were used together with calculated conversion coefficients to extract reduced transition probabilities for all the isomeric transitions established in the present work. The results can be found in Table VII.

IV. DISCUSSION

A. Systematics

The systematics of the excitation energies of the main yrast levels are presented in Fig. 18 for the chain of even, $A = 116$–130, Sn isotopes. The 2_1^+ state energy in ^{132}Sn has been added to the figure to illustrate the $N = 82$ shell closure. A smooth, regular behavior as a function of A can be seen for all the states included: This observation provides confidence in the identifications and spin-parity assignments proposed as

TABLE VII. Reduced transition probabilities $B(E\lambda)$, in (e^2 fm$^{2\lambda}$) and in Weisskopf units, extracted in the present study for the $E1$, $E2$, and $E3$ transitions observed in decays of the 15^- and 13^- isomeric states in $^{120-128}$Sn. In column 5, the percentage intensity of the respective decay branches is given with calculated electron conversion [20] taken into account (see text for details).

	E_γ (keV)	$I_i \to I_f$	$T_{1/2}$ (ns)	branching (%)	$B(E\lambda)$ (e^2 fm$^{2\lambda}$)	$B(E\lambda)$ (W.u.)
^{120}Sn	241.7	$15^- \to 13^-$, $E2$	30(3)	93.2(46)	21(2)	0.60(6)
	253.2	$13^- \to 11^-$, $E2$	4(1)	26.1(26)	36(10)	1.0(3)
	556.9	$13^- \to 12^+$, $E1$		72.2(43)	$4.6(12) \times 10^{-7}$	$2.9(8) \times 10^{-7}$
^{122}Sn	242.5	$15^- \to 13^-$, $E2$	134(12)	93.3(28)	4.7(4)	0.13(1)
	70.2	$13^- \to 11^-$, $E2$	40(3)	0.58(13)	49(12)	1.4(3)
	264.5	$13^- \to 11^-$, $E2$		12.5(19)	1.4(2)	$3.9(6) \times 10^{-2}$
	609.6	$13^- \to 12^+$, $E1$		80.0(39)	$3.9(3) \times 10^{-8}$	$2.3(8) \times 10^{-8}$
	1712.8	$13^- \to 10^+$, $E3$		2.9(10)	20(7)	$2.3(2) \times 10^{-2}$
^{124}Sn	228.8	$15^- \to 13^-$, $E2$	260(30)	91.9(28)	3.2(4)	$8.7(11) \times 10^{-2}$
	251.1	$13^- \to 11^-$, $E2$	6.7(9)	14.8(20)	13(2)	0.35(5)
	620.1	$13^- \to 12^+$, $E1$		84.1(40)	$2.3(3) \times 10^{-7}$	$1.4(2) \times 10^{-7}$
^{126}Sn	180.8	$15^- \to 13^-$, $E2$	114(12)	83.5(25)	22(2)	0.59(5)
	240.5	$13^- \to 11^-$, $E2$	$\leqslant 3$	17.7(20)	$\geqslant 42$	$\geqslant 1.1$
	571.0	$13^- \to 12^+$, $E1$		80.8(49)	$\geqslant 6.3 \times 10^{-7}$	$\geqslant 3.9 \times 10^{-7}$
^{128}Sn	119.7	$15^- \to 13^-$, $E2$	220(30)[a]	54.3(16)	57(8)	1.5(2)

[a]Value taken from Ref. [12].

a result of the analysis described above. The 2_1^+ energies are remarkably stable throughout the isotopic chain: A shallow minimum appears for ^{124}Sn, accompanied by a surprisingly symmetric energy increase when moving away from this mass number on either side. This shallow minimum is a signature for the half-filling of the $\nu h_{11/2}$ subshell at $A = 124$. In contrast to this stability of the 2_1^+ excitations, all other, higher-lying states display a rather smooth decrease of their excitation energies with A. This regular behavior had been established earlier for the $\nu = 2$ seniority states represented here by the 7^- and 10^+ levels. In Fig. 18, the 5^- level energies are also included to display the energy inversion with respect to the 7^- state

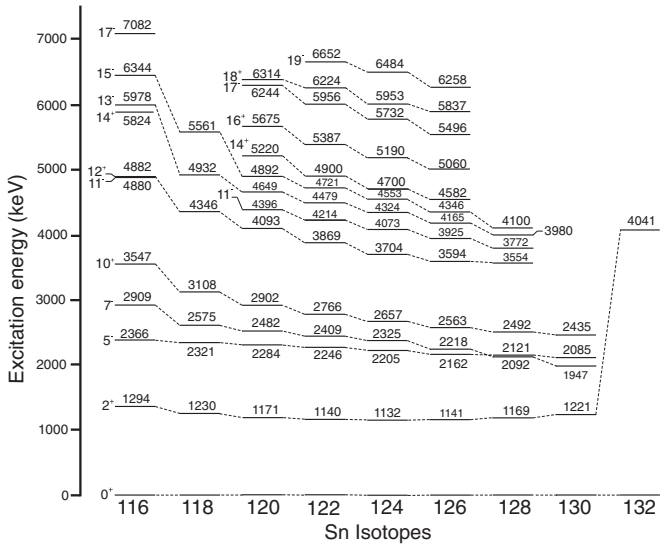

FIG. 18. Systematics of energies of yrast levels established in neutron-rich even Sn isotopes. The ^{132}Sn, 2^+ energy is indicated to highlight the $N = 82$ shell closure. For the sake of clarity, not all the observed and assigned states are included.

occurring at ^{128}Sn which reflects the change of the position of the Fermi level relative to the $s_{1/2}$ and $d_{3/2}$ orbitals. For the $\nu = 4$ seniority excitations, represented here by both positive- (12^+, 14^+, 16^+) and negative- (11^-, 13^-, 15^-) parity states, the systematic decrease is even more pronounced and includes that of the 12^+ state, where the $12^+ \to 10^+$ transition energy also decreases in contrast to the noted stability for the $2_1^+ \to 0^+$ ones mentioned above. The 17^-, 18^+, and 19^- levels, selected here to represent the seniority $\nu = 6$ excitations, display a similarly regular decrease and, as a general consequence of this behavior, the yrast sequences in the even Sn isotopes become increasingly compressed in energy with mass. It should be noted that, as discussed in Sec. III A, the 13^- and 15^- levels in ^{118}Sn were tentatively assigned on the basis of the observed regularity in the level systematics. Moreover, one should keep in mind that the yrast levels in ^{118}Sn and, in particular, in ^{116}Sn (which were taken from other studies [21] and are included in Fig. 18) should naturally represent more complex structures involving more of the $\nu d_{5/2}$ and $\nu g_{7/2}$ neutron orbitals than is the case for heavier isotopes. For obvious reasons, the systematics show only seniority-2 states in the two-hole ^{130}Sn isotope and seniority-2 and -4 states in the four-hole ^{128}Sn nucleus. In the latter case, the 14^+ and 16^+ levels have not yet been identified.

B. Shell-model calculations

Shell-model calculations have been carried out for all even, $A = 122$–130, Sn isotopes with the OXBASH shell-model code [22]. These calculations assume ^{132}Sn as a closed core and use a valence space where the neutron holes occupy the $\nu(0g_{7/2}, 1d_{5/2}, 1d_{3/2}, 2s_{1/2}, 0h_{11/2})$ orbitals. The respective single-particle energies were taken such that the ^{131}Sn experimental values of -9.74, -8.97, -7.31, -7.62, and -7.38 MeV are reproduced [23,24]. For the set of two-body matrix elements (TBMEs), the neutron-neutron part of the shell-model interaction presented in Ref. [25] was used.

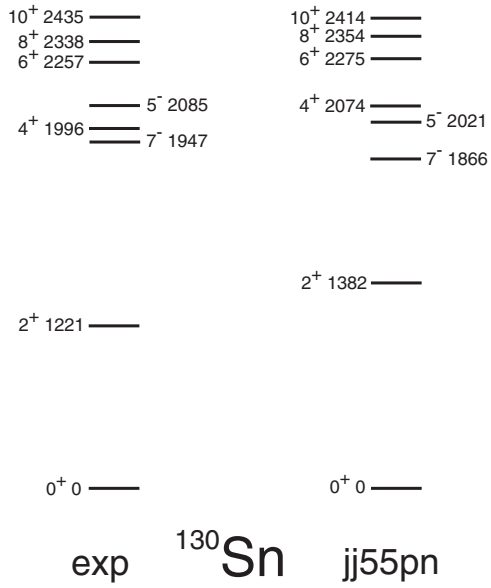

FIG. 19. Experimental and calculated levels in ^{130}Sn.

This interaction was obtained starting from the CD-Bonn nucleon-nucleon potential [26], and the G-matrix method was used to arrive at the renormalized interaction. Subsequently, the effective interaction for the valence space was derived with the $\hat{Q}$-box method, and it included all nonfolded diagrams up to the third order in the interaction G while summing up the folded diagrams to infinite order [27]. Finally, all the TBMEs had to be multiplied by a factor of 0.9 to achieve a satisfactory agreement between experiment and calculations for ^{130}Sn. Hereafter, the results of the shell-model calculations are labeled with the jj55pn symbol.

Comparisons between the experimental (exp) and calculated (jj55pn) levels in ^{130}Sn and ^{128}Sn are presented in Figs. 19 and 20, respectively: They provide an indication of the type of agreement between data and theory that can be expected for the lighter Sn isotopes. For the simplest case of the two-neutron-hole ^{130}Sn nucleus, the agreement reflects, in essence, the adjustments made in the calculations to the values of the TBMEs discussed above. However, the comparison displayed in Fig. 20 for the four-neutron-hole ^{128}Sn isotope indicates that differences in the range of 100 keV or more between experimental and calculated energies should not be viewed as surprising. Similar comparisons for ^{126}Sn, ^{124}Sn, and ^{122}Sn are found in Figs. 21, 22, 23, i.e., in order of increasing complexity in the calculations. Similar results cannot be presented for the lightest Sn isotopes under discussion as the required computing time was prohibitive. In general, satisfactory agreement is observed between the calculated and the experimental spectra up to the highest spins. Taking into account a systematic mismatch for the positive-parity levels, where the computed states are often about 200 keV lower than their experimental counterparts, the calculations strongly support the spin-parity assignments inferred from the available data for most states. Apart from the ^{130}Sn case, only the 7^-, 8^+, and 10^+ highest-spin levels are shown for seniority $\nu = 2$ states and these display good agreement

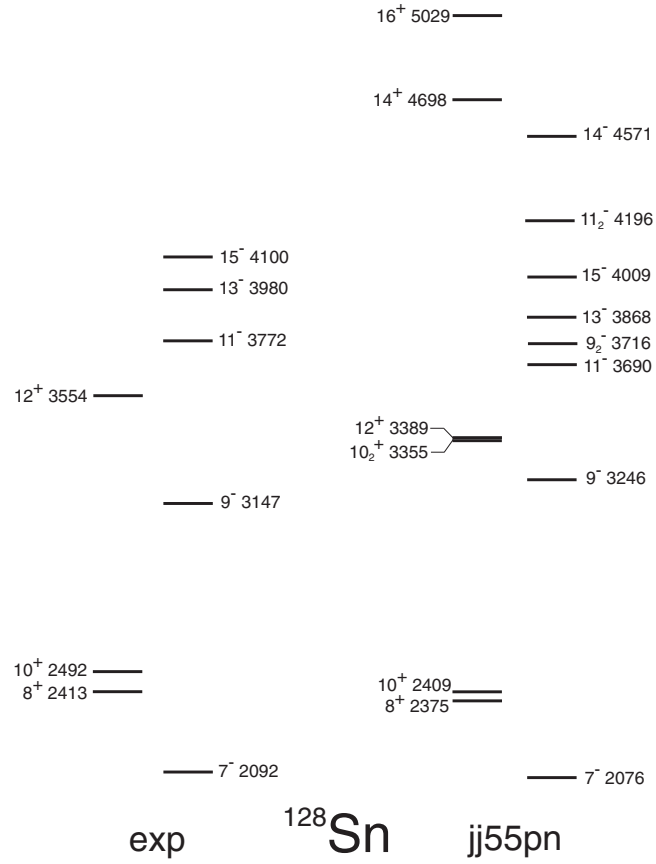

FIG. 20. Comparison of the ^{128}Sn level energies established in the experiment with the jj55pn shell-model calculations described in the text. The negative- and positive-parity levels are displaced with respect to each other for the sake of clarity.

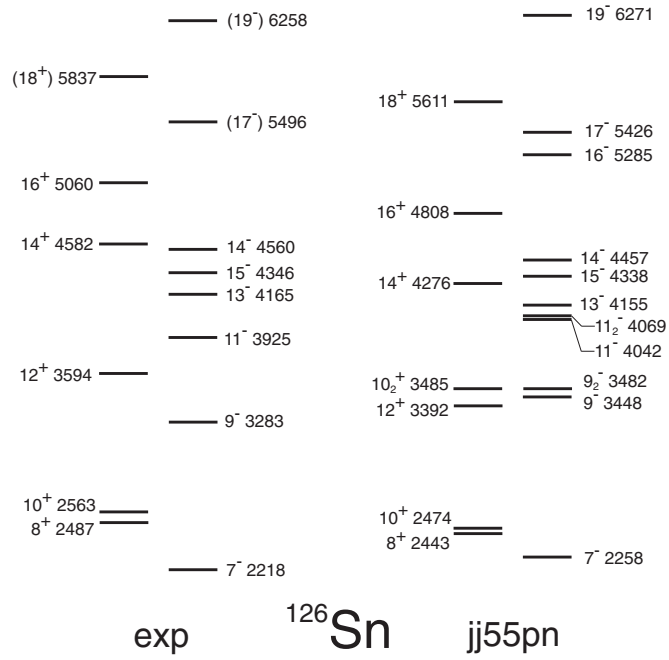

FIG. 21. Same as in Fig. 20, but for the ^{126}Sn isotope.

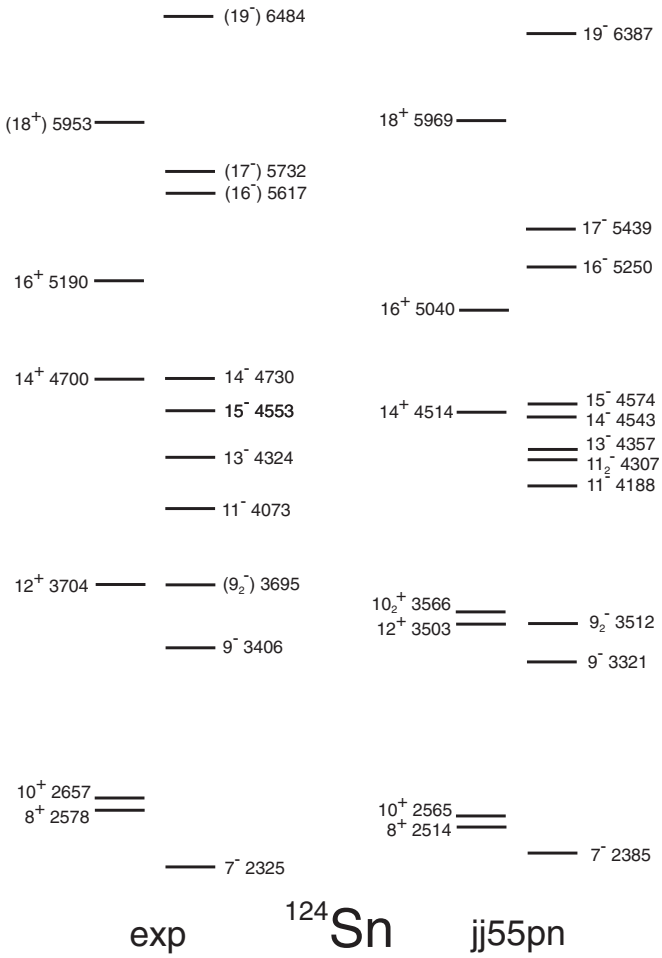

FIG. 22. Same as in Fig. 20, but for the ^{124}Sn isotope.

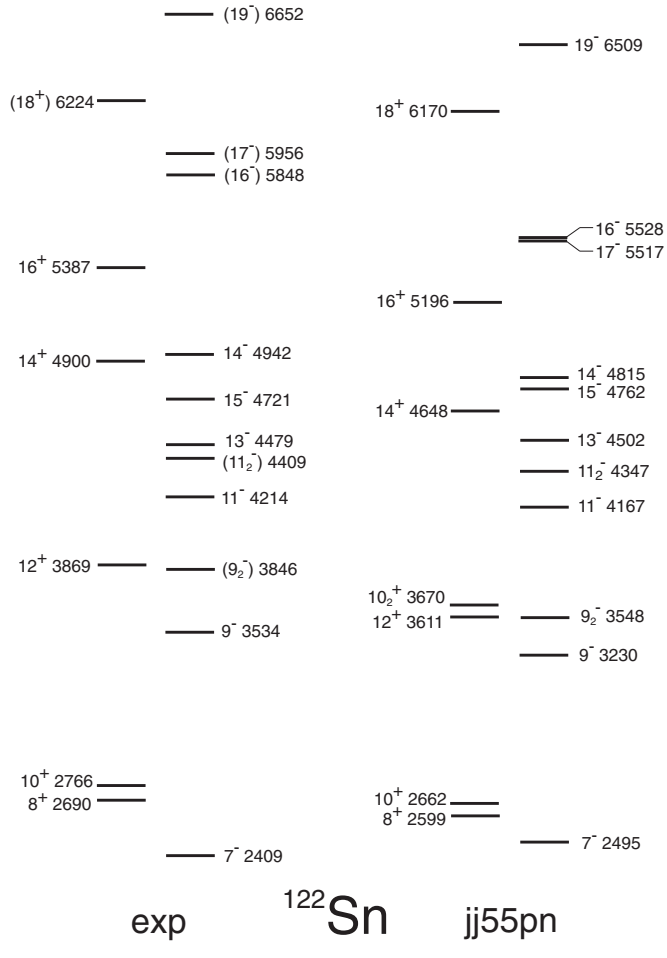

FIG. 23. Same as in Fig. 20, but for the ^{122}Sn isotope.

between experiment and calculations. The calculated wave functions indicate predominant (close to 100%) amplitudes for the $\nu(h_{11/2}d_{3/2})$ configuration in the 7^- state and of the $\nu(h_{11/2})^2$ one in the 10^+ and 8^+ levels. In each isotope, the remaining paired neutron holes are distributed over all the available orbitals in the model space, reaching the most bound $d_{5/2}$ and $g_{7/2}$ orbitals for which the total occupation increases from 14% in ^{128}Sn to 25%, 37%, and 45% in ^{126}Sn, ^{124}Sn, and ^{122}Sn, respectively. Whereas the results of the calculations do not allow one to distinguish unpaired two-neutron holes when they occupy the same orbital, they point to very small amplitudes for the wave functions involving single holes placed in different orbitals. In the structure of the 10^+ and 8^+ states, the sum of such amplitudes amounts to only 2% in ^{128}Sn and 3% in ^{126}Sn, and such configurations are practically absent in the lighter isotopes. Thus, the calculations support the view that contributions of higher-seniority excitations to the seniority $\nu = 2$ states are small.

With the noted good general agreement between experimental and calculated seniority $\nu = 2$ levels, a more detailed inspection indicates that the calculated 10^+ states are systematically lower by $\sim$100 keV than the 10^+ isomeric levels seen in the data. At the same time, the calculated 7^- states are also slightly lower in energy in ^{130}Sn and ^{128}Sn by 81 and 16 keV, respectively, but a systematic small upward shift is observed for ^{126,124,122}Sn ($\Delta E = 40$, 60, and 86 keV). The trends of these small, but systematic, differences between experimental and calculated 7^- and 10^+ level energies suggest that this minor disagreement does not arise from a problem with the calculated ground-state energies. Rather, it is likely that further small modifications to the two-body interactions need to be considered in future attempts to improve the agreement. This is seen more clearly when comparing the experimental and calculated seniority $\nu = 4$ states. The 12^+, 14^+, and 16^+ levels are the most prominent $\nu(h_{11/2})^4$ seniority $\nu = 4$ states and they are calculated systematically about 200 keV lower in energy than their experimental counterparts. Their wave functions are complex and also involve additional 0^+ couplings with the neutron-hole pairs distributed over other available orbitals. Among these positive-parity states, the maximally aligned spin 16^+ levels have the largest amplitudes for the $\nu(h_{11/2})^4$ configuration: These amount to 99%, 70%, 59%, and 53% in the $^{128-122}$Sn even isotopes. In fact, only in the case of ^{126}Sn do the calculations indicate an 8% contribution to the amplitude of the 16^+ level originating from a configuration involving unpaired $s_{1/2}$ and $d_{3/2}$ neutron holes. However, in every isotope, the yrast, negative-parity levels, which arise predominantly from the coupling of the $(h_{11/2})^3$ and $d_{3/2}$ or

$s_{1/2}$ neutrons, are calculated to lie closer to the corresponding data. This observation holds especially when considering the yrast 15^- and 13^- isomeric states, which are expected to be associated with the simplest intrinsic structure. Wave functions of the maximum-spin 15^- levels indeed indicate a predominant $\nu(h_{11/2})^3 d_{3/2}$ configuration with respective amplitudes calculated to be 97%, 84%, 62%, and 52% in $^{128-122}$Sn. At the same time, the configurations of the 13^- state, with the exception of ^{128}Sn, involve more contributions from the $s_{1/2}$ orbital. For the four $^{128-122}$Sn isotopes, the calculated wave functions indicate contributions of 84%, 19%, 15%, and 12% to the amplitudes from the $\nu(h_{11/2})^3 d_{3/2}$ configuration and 12%, 53%, 35%, and 30% for the $\nu(h_{11/2})^3 s_{1/2}$ one. However, as discussed below, this predominance of the $s_{1/2}$ orbital in the calculated wave functions of the 13^- levels leads to difficulties in providing a straightforward interpretation for the $B(E2)$ values of the isomeric $15^- \rightarrow 13^-$, $E2$ transitions.

For negative-parity levels of lower spin, two doublets of 9^- and 11^- states are predicted and one would expect to observe these in the present experiment. However, only single 9^- and 11^- levels were established in ^{128}Sn (Fig. 20) and in ^{126}Sn (Fig. 21), while a pair of 9^- states and single 11^- level are seen in ^{124}Sn (Fig. 22). In ^{122}Sn, however (Fig. 23), both 9^- and 11^- doublets are present in the data with energies close to the computed ones. According to the calculations, the wave functions for these states vary significantly throughout the isotopic chain. In ^{128}Sn, the two 9^- states have significantly different structures, with the $\nu(h_{11/2})^3 d_{3/2}$ configuration dominating in the 9^-_1 level with an 86% amplitude while the seniority $\nu = 2$ $(g_{7/2}h_{11/2})$ one prevails with an 89% amplitude in the 9^-_2 state computed to be 0.5 MeV higher in excitation energy. In the lighter isotopes, the calculated states are closer in energy and their intrinsic structure is more complex. However, a clear tendency is present to reverse the composition calculated for ^{128}Sn. In ^{126}Sn, the seniority $\nu = 4$ $(h_{11/2})^3 d_{3/2}$ amplitude decreases to 59% in the 9^-_1 state and increases to 22% in the 9^-_2 level. At the same time, the seniority $\nu = 2$ $(g_{7/2}h_{11/2})$ configuration is present with a 9% amplitude in the 9^-_1 level and has a 40% amplitude in the 9^-_2 state, lower by a factor of roughly 2 compared to ^{128}Sn. In the lighter ^{124}Sn and ^{122}Sn isotopes, the seniority $\nu = 4$ configuration dominates the higher-lying 9^-_2 state with 65% and 52% respective amplitudes, while the lower 9^-_1 level is associated mainly with the $\nu = 2$ excitation involving the $g_{7/2}$ orbital. The two 11^- levels are seniority $\nu = 4$ excitations of rather similar composition, differing mainly by the spin coupling of the three $h_{11/2}$ neutron holes to an unpaired hole placed in another of the available orbitals. In ^{128}Sn, the 11^-_1 and 11^-_2 states are calculated with 82% and 86% respective amplitudes for the $(h_{11/2})^3 d_{3/2}$ configuration and 10% for the $(h_{11/2})^3 s_{1/2}$ one. In the lighter isotopes, the calculated wave functions become increasingly fragmented with a fast decrease in the amplitudes of configurations involving the $\nu d_{3/2}$ orbital.

The 14^- level observed in ^{122,124,126}Sn is of particular interest: In the three isotopes, it is located roughly 200 keV above the 15^- isomer, an observation only partly reproduced by the jj55pn calculations, as the latter predict an even smaller energy difference between the two states or computes the 14^- level below the 15^- isomer (in ^{124}Sn). In every case, the 14^- level decays solely through an $M1$ transition to the 15^- isomer and a possible competing $M1$ branch to the lower-lying 13^- level remains unobserved. In every instance, the estimated upper limit of the $14^- \rightarrow 13^-$ transition intensity, combined with the difference in the E_γ^3 energy factors for the two competing $M1$ branches, leads to a $B(M1)$ reduced transition probability that is at least 15 times smaller for the branch to the 13^- state than for the observed $M1$ transition to the 15^- level. Generally, the wave functions of calculated nonyrast states are complex with, for example, non-negligible amplitudes for configurations involving paired neutron holes scattered over the entire model space of single-particle levels. Nevertheless, the 14^- and, especially, as discussed above, the 15^- levels in ^{122,124,126}Sn are predominantly arising from the $(h_{11/2})^3 d_{3/2}$ coupling while the $(h_{11/2})^3 s_{1/2}$ configuration dominates the structure of the 13^- states. In the calculated wave functions of the 14^- states, the dominance of the $(h_{11/2})^3 d_{3/2}$ configuration is reflected by 93%, 71%, 42%, and 28% amplitudes in ^{128,126,124,122}Sn, respectively, whereas the $(h_{11/2})^3 s_{1/2}$ contribution remains in a range of 10% in all isotopes. Thus, a one-time forbidden $d_{3/2} \rightarrow s_{1/2}$ transition could possibly account for the absence of a $14^- \rightarrow 13^-$ $M1$ branch.

The interpretation of highest-lying states with seniority $\nu = 6$ and spins larger than the 16^+ and 15^- values available for seniority $\nu = 4$ levels is less transparent. This is attributable in part to the tentative character of the proposed spin-parity assignments as well as to the expected limited accuracy of the jj55pn calculations in this domain. Nevertheless, in the ^{122,124,126}Sn isotopes, the experimental yrast levels tentatively assigned as 18^+ fit surprisingly well with the computed ones: Data and calculations are 54 keV apart in ^{122}Sn, only 16 keV apart in ^{124}Sn, and 226 keV apart in ^{126}Sn. The calculated wave functions indicate that, in ^{126}Sn, the two units of spin above the yrast 16^+ level come mostly from the pair of $d_{3/2}$ holes (69% amplitude) while, in ^{122,124}Sn, the $(h_{11/2})^6$ configuration dominates with amplitudes of 43% and 20%, respectively. Also, for the negative-parity 17^- and 19^- yrast states, the calculated counterparts reproduce the data fairly well. For the 19^- state, the energy differences between data and calculations are 14, 97, and 143 keV in ^{126}Sn, ^{124}Sn, and ^{122}Sn, respectively, while they are 70, 293, and 439 keV for the 17^- levels with the calculations systematically under predicting the observations in this case. Interestingly, in the ^{124}Sn and ^{122}Sn isotopes, the nonyrast 16^- levels calculated to lie close in energy to the respective 17^- levels appear to have been observed as well.

The comparisons presented in Figs. 21, 22, and 23 have been restricted to instances where a reasonably clear correspondence could be made between the data and the results of the calculations. Many more levels have been established in the present work: their interpretation requires additional, qualitative progress in the experimental input combined with significant improvements in the accuracy of the calculations. Nevertheless, it is worth noting that the present jj55pn calculations limit the maximum spin values achievable to $I = 21$, $I = 21$, and $I = 22$ for the highest-energy levels observed in this experiment at 8.4 MeV in ^{126}Sn, 7.5 MeV in ^{124}Sn, and 8.7 MeV in ^{122}Sn, respectively.

C. Transition probabilities

The measured half-lives of the long-lived states established in the present work were used together with the observed decay branchings to extract reduced transition probabilities for the isomeric transitions. The relevant numerical values are listed in Table VII. They result in the transition amplitudes displayed in Fig. 24. For completeness, a set of $B(E2)$ values established earlier in a series of experiments for the seniority $\nu = 2$ and 3 isomers [3–7] is displayed (in terms of amplitudes) in the lower part of Fig. 24(a). Here, a geometrical factor of 0.514 [7] was used to renormalize the $B(E2)$ amplitudes of the $27/2^- \rightarrow 23/2^-$ transitions in the odd-Sn isotopes so that they can readily be compared with the values for of the $10^+ \rightarrow 8^+$ transitions in the even Sn nuclei. It should be pointed out that the convention introduced in Refs. [3–7] was adopted here as well; i.e., $B(E2)$ amplitudes are shown rather than the $B(E2)$ values, and the positive sign is assigned to the amplitudes of the light Sn isotope with a change to negative values when the $B(E2) = 0$ line is crossed. In earlier work, the observed nearly linear decline as a function of mass A of the $B(E2)$ amplitudes, with an average slope of $-0.83\ e\ \mathrm{fm}^2/A$, was viewed as a striking demonstration of the shell-model interpretation of isomeric states in neutron-rich Sn isotopes [4–6].

In the same manner, in the upper part of Fig. 24(a), the $B(E2)$ amplitudes are displayed for $E2$ transitions observed in the decays of the 15^- and 13^- isomers established in the present work. It is noteworthy that, for these seniority $\nu = 4$ isomers, the $B(E2)$ transition amplitudes display a behavior similar to that exhibited by transitions involving the seniority $\nu = 2,3$ states. In this case, the linear decrease of the $B(E2)$ amplitudes defines a similar average slope of $-0.78\ e\ \mathrm{fm}^2/A$ for the $15^- \rightarrow 13^-$ transitions and a slightly faster decline of $-1.03\ e\ \mathrm{fm}^2/A$ for the $13^- \rightarrow 11^-$ ones. In the case of the $B(E2; 13^- \rightarrow 11^-)$ amplitudes, data are available for the $^{120-124}$Sn isotopes only, although the upper limit determined for ^{126}Sn from the estimated half-life is in line with the linear decrease with A. Surprisingly, the values of the $B(E2)$ amplitudes determined for the $15^- \rightarrow 13^-$ and $13^- \rightarrow 11^-$ transitions are of the same magnitude as those obtained for the seniority $\nu = 2,3$ states, when the same geometrical reduction factor of 0.514 is used to account for the main contribution of the $(h_{11/2})^3$ couplings in the intrinsic structure of these states. It should be noted that, as stated above, a simple interpretation based on the analogy with the $B(E2)$ values observed for the seniority $\nu = 3$, $27/2^- \rightarrow 23/2^-$ isomeric decays in odd-Sn isotopes is in conflict with the structure of the calculated 13^- states discussed above. Indeed, this noted similarity in $B(E2)$ values between odd and even nuclei would, at first sight, imply that the decays are governed by the change in the $h_{11/2}$ couplings and would require the configurations of both the 15^- and 13^- to include an odd $d_{3/2}$ neutron acting as a spectator. However, while the $(h_{11/2})^3 d_{3/2}$ configuration dominates the 15^- levels in the jj55pn calculations, the 13^- levels are of main $(h_{11/2})^3 s_{1/2}$ character and the straightforward interpretation using the analogy no longer holds. Yet, it should also be recognized that a preferred $(h_{11/2})^3 d_{3/2}$ structure for the 13^- state would also account in a satisfactory manner for the

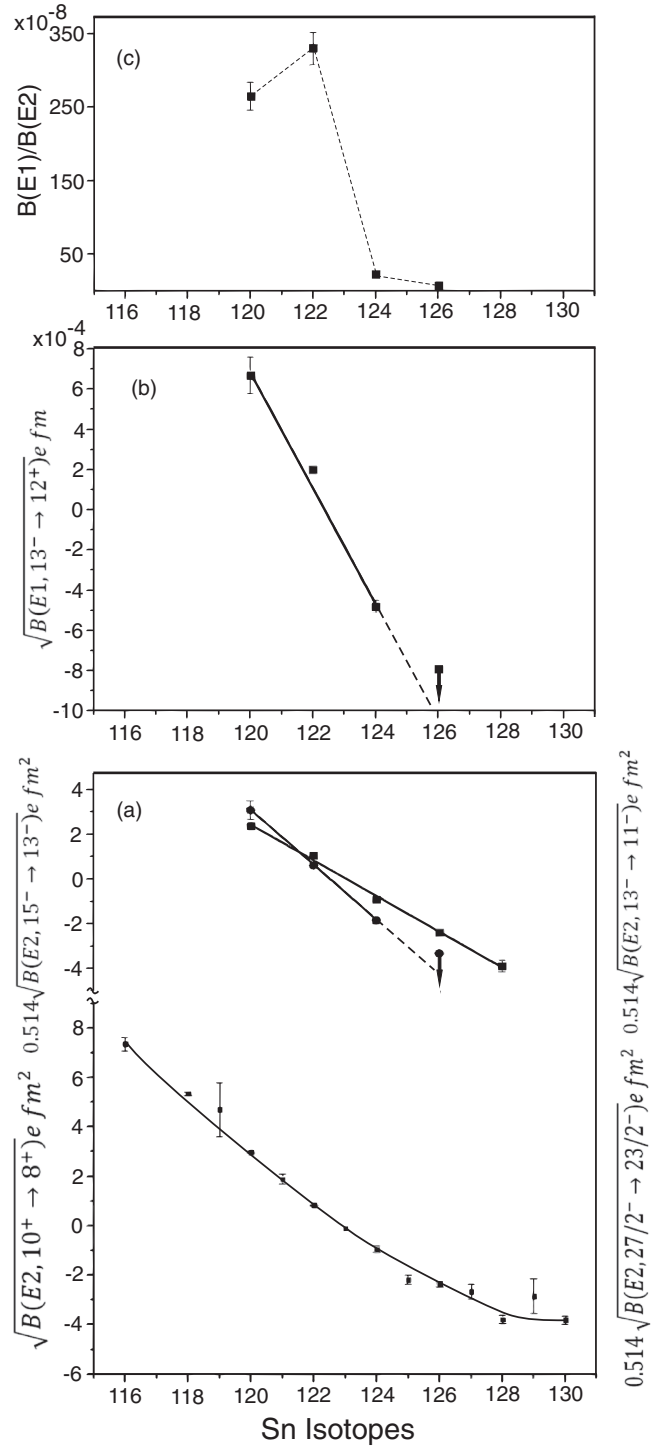

FIG. 24. Transition amplitudes for isomeric decays observed in the Sn isotopes as calculated from the reduced transition rates of Table VII. In panel (a), the $E2$ amplitudes for transitions associated with the 15^- (squares) and 13^- (circles) isomeric decays are displayed and compared with a complete set of $E2$ transition amplitudes known for the $(h_{11/2})^n$ isomers in Sn isotopes (lower points). In panel (b), $E1$ transition amplitudes are displayed for the main $E1$ branches established in the 13^- isomer decays. In panel (c), the $B(E1)/B(E2)$ ratios of reduced transition probabilities (normalized to Weisskopf units) are displayed for the $E1$ and $E2$ branches observed in the decays of 16^+ states in the respective Sn isotopes. (see text).

branching in the decay of the 14^- level discussed above, as the absence of the $14^- \rightarrow 13^-$, $M1$ transition would be a natural consequence of the $27/2^-$ and $23/2^-$ $(h_{11/2})^3$ couplings in the two states involved. It is likely that those observations reflect shortcomings of the calculations, and it is hoped that this issue will be resolved in the future by an improved shell-model approach.

The intense $E1$ transitions feeding the yrast 12^+ states represent the main decay branch out of the 13^- isomers. All of these are strongly retarded $E1$ transitions ($<10^{-6}$ W.u.; see Table VII) and the extracted $B(E1)$ amplitudes are displayed in Fig. 24(b). With the three data points for ^{120,122,124}Sn and the upper limit derived for ^{126}Sn, an obvious trend of linear decrease with mass is observed with a fitted slope coefficient of -2.88×10^4 e fm/A. Although this slope value only defines quantitatively the decrease, the regularity of the observed behavior with A is quite remarkable, as it mirrors rather closely that discussed above for the $E2$ transition amplitudes. Usually, retarded $E1$ transitions proceed via small admixtures in the wave functions of the initial and final states involved, and the $B(E1)$ values are expected to exhibit a large scatter as a result. Hence, the regular decrease with A can hardly be understood at present and the possibility that the observation is accidental cannot (yet) be ruled out. In this general context, it is also worth remembering that the relatively long half-life of the 13^- isomer in ^{122}Sn enabled the observation of additional, much weaker, deexcitation paths. The 70-keV $E2$ branch feeding the second 11^- state is apparently much faster than the other $E2$ transitions known in this isotope (see Table VII). Also unique to the ^{122}Sn isotope is the observation of a $13^- \rightarrow 10^+$, $E3$) branch with a rate close to 10^{-3} W.u. These observations remain a challenge for theory to explain.

An additional regularity in the change in transition rates with mass was observed within the neutron-rich Sn isotopes under investigation: The 16^+ yrast states established in the four $^{120-126}$Sn isotopes decay via $E2$ transitions to their respective lower-lying 14^+ levels and by competing $E1$ branches to the 15^- isomeric states. It is apparent that the intensity of the $E1$ decays varies over the isotopic chain: It is the dominant deexcitation mode out of the ^{120}Sn 16^+ level, but becomes gradually less important in the heavier isotopes. An upper limit was obtained in ^{126}Sn and the competing $E2$ branch was the only one observed. Although the corresponding $E1$ and $E2$ transition rates could not be determined, because the 16^+ states were found to have half-lives shorter than 3 ns, the quantitative illustration of the observations is displayed in Fig. 24(c). Using the energies and intensities of the respective $E1$ and $E2$ transitions observed in the data, the $B(E1)/B(E2)$ ratios of reduced transition rates [in Weisskopf units] were calculated for $^{120-126}$Sn as $265(19) \times 10^{-8}$, $329(22) \times 10^{-8}$, $24(3) \times 10^{-8}$, and $\leqslant 8 \times 10^{-8}$, respectively. Taking into account the regularity in the A dependence of the $B(E2)$ values for other $E2$ transitions established above, a similar behavior may be expected for the $16^+ \rightarrow 14^+$, $E2$ transitions and, consequently, the $B(E1)/B(E2)$ ratios of Fig. 24(c) seem to indicate that, in general, the $E1$ transition rates decrease much faster with A than the $E2$ ones. It is possible that the irregularity observed for ^{122}Sn is resulting from the small offset of the point where $B(E1)$ and $B(E2)$ amplitudes cross the zero line. Assuming that this explanation is correct leads to an observed decreasing trend that appears to be consistent with the result of Fig. 24(b) and suggests that the contributions of small wave-function admixtures responsible for the rates of retarded $E1$ transitions behave fairly smoothly with the increasing mass number.

V. CONCLUSIONS

High-spin states above the previously known 10^+ isomers have been investigated in the neutron-rich, even $^{118-128}$Sn isotopes produced using three heavy-ion-induced fusion-fission reactions with different projectile-target combinations. By exploiting delayed- and cross-coincidence techniques, extensive level schemes have been delineated. They are dominated by seniority $\nu = 4$ and 6 excitations. The decay from newly established 15^- and 13^- isomeric states through parallel pathways toward the lower-lying 10^+ and 7^- isomers enabled the assignment of unique spin-parity values to nearly all of the observed seniority $\nu = 4$ states. To some of the higher-lying, seniority $\nu = 6$ levels, spin-parity values could be tentatively assigned as well. Shell-model calculations performed for all even neutron-rich Sn isotopes down to $A = 122$ gave results mostly consistent with the experimental observations and reproduced the measured level energies with satisfactory accuracy.

The systematics of the level energies throughout the isotopic chain of neutron-rich Sn isotopes investigated here displays a striking regular dependence with mass and this smooth behavior adds further confidence in the experimental results. Even more striking is the regularity observed in the variation of the reduced transition probabilities extracted from the measured isomeric half-lives for a number of $E2$ and $E1$ transitions observed in the decays of the new 15^- and 13^- isomers. For these $E2$ transitions, the extracted $B(E2)$ probabilities have similar values and follow rather precisely the A dependence established earlier for the $(h_{11/2})^n$, seniority $\nu = 2,3$ isomers in the full range of $^{116-130}$Sn. At the same time, the observed smooth decrease with A of the $B(E1)$ transition probabilities suggests that even small admixtures in the wave-function amplitudes responsible for these strongly retarded $E1$ transitions vary in a fairly smooth way with changing mass. These noted regularities indicate that improvements of the shell-model calculations should be possible by taking into account the guidance provided by the full range of experimental results. In a forthcoming publication, the results obtained from the same experiments for the neutron-rich odd-A Sn isotopes will be presented and attempts to improve the shell-model calculations will be discussed.

ACKNOWLEDGMENTS

The authors thank the ATLAS operating staff for the efficient running of the accelerator and J. P. Greene for target preparations. We are indebted to B. A. Brown for providing the nucleon-nucleon interactions. This work was supported by the Polish National Science Center, Projects No. UMO-2012/07/N/ST2/02861 and No. NN202-

008640, the US Department of Energy, Office of Nuclear Physics, under Contract No. DE-AC02-06CH11357 (ANL) and Grant No. DE-FG02-94ER40834 (UM), as well as by the Marian Smoluchowski Krakow Research Consortium "Matter-Energy-Future" as a Leading National Center (KNOW).

[1] M. Ogawa, R. Broda, K. Zell, P. J. Daly, and P. Kleinheinz, Phys. Rev. Lett. **41**, 289 (1978).
[2] P. J. Daly *et al.*, Z. Phys. A **298**, 173 (1980).
[3] M. Ishihara, R. Broda, and B. Herskind, in *Proceedings of the International Conference on Nuclear Physics, Munich*, edited by J. de Boer and H. J. Mang (North-Holland, Amsterdam, 1973), Vol. 1, p. 256.
[4] R. Broda *et al.*, Phys. Rev. Lett. **68**, 1671 (1992).
[5] R. H. Mayer *et al.*, Phys. Lett. B **336**, 308 (1994).
[6] C. T. Zhang, P. Bhattacharyya, P. J. Daly, Z. W. Grabowski, R. Broda, B. Fornal, and J. Blomqvist, Phys. Rev. C **62**, 057305 (2000).
[7] S. Lunardi, P. J. Daly, F. Soramel, C. Signorini, B. Fornal, G. Fortuna, A. M. Stefanini, R. Broda, W. Męczyński, and J. Blomqvist, Z. Phys. A **328**, 487 (1987).
[8] J. H. McNeill, J. Blomqvist, A. A. Chishti, P. J. Daly, W. Gelletly, M. A. C. Hotchkis, M. Piiparinen, B. J. Varley, and P. J. Woods, Phys. Rev. Lett. **63**, 860 (1989).
[9] Y. H. Chung *et al.*, Phys. Rev. C **29**, 2153 (1984).
[10] N. Fotiades, M. Devlin, R. O. Nelson, J. A. Cizewski, R. Krücken, R. M. Clark, P. Fallon, I. Y. Lee, A. O. Macchiavelli, and W. Younes, Phys. Rev. C **84**, 054310 (2011).
[11] A. Astier *et al.*, Phys. Rev. C **85**, 054316 (2012).
[12] S. Pietri *et al.*, Phys. Rev. C **83**, 044328 (2011).
[13] Ł. W. Iskra *et al.* (unpublished).
[14] R. Broda *et al.*, Phys. Rev. C **86**, 064312 (2012).
[15] W. Królas *et al.*, Phys. Rev. C **84**, 064301 (2011).
[16] R. Broda *et al.*, Phys. Rev. C **82**, 034319 (2010).
[17] R. Broda, J. Phys. G: Nucl. Part. Phys. **32**, R151 (2006).
[18] I. Y. Lee, Nucl. Phys. A **520**, 641c (1990).
[19] Ł. W. Iskra *et al.*, Acta Phys. Pol. B **44**, 395 (2013).
[20] T. Kibédi *et al.*, Nucl. Instrum. Methods Phys. Res., Sect. A **589**, 202 (2008).
[21] A. Savelius *et al.*, Nucl. Phys. A **637**, 491 (1998).
[22] B. A. Brown, A. Etchegoyen, N. S. Godwin, W. D. M. Rae, W. A. Richter, W. E. Ormand, E. K. Warburton, J. S. Winfield, L. Zhao, and C. H. Zimmerman, OXBASH for Windows, MSU-NSCL Report 1289, 2004.
[23] R. B. Firestone, V. S. Shirley, C. M. Baglin, S. Y. Frank Chu, and J. Zipkin, *Table of Isotopes*, 8th ed. (Wiley Interscience, New York, 1996).
[24] B. Fogelberg *et al.*, Phys. Rev. C **70**, 034312 (2004).
[25] B. A. Brown, N. J. Stone, J. R. Stone, I. S. Towner, and M. Hjorth-Jensen, Phys. Rev. C **71**, 044317 (2005).
[26] R. Machleidt, F. Sammarruca, and Y. Song, Phys. Rev. C **53**, R1483 (1996).
[27] M. Hjorth-Jensen, T. T. S. Kuo, and E. Osnes, Phys. Rep. **261**, 125 (1995).